Int. J. Multiphase Flow Vol. 17, No. 6, pp. 717–744, 1991
Printed in Great Britain.

0301-9322/91 $3.00 + 0.00

SEPARATION OF SCREW-SENSED PARTICLES IN A HOMOGENEOUS SHEAR FIELD

Y.-J. KIM and W. J. RAE
Department of Mechanical and Aerospace Engineering, State University of New York at Buffalo, Buffalo, NY 14260, U.S.A.

(Received 3 October 1990; in revised form 8 July 1991)

Abstract—The Stokes motions of three-dimensional screw-sensed slender particles in a homogeneous shear field are investigated, including the effects of buoyancy. Conclusions are drawn about the possibility of achieving a separation of mixtures of right- and left-handed particles. The linearity of the Stokes equations allows complex flows to be solved by adding the effects of the several terms which describe the flow in which the particle is immersed. The homogeneous shear flow considered here consists of three such terms; solutions for a series of 12 unit motions are sufficient to determine the hydrodynamic resistance tensors. The forces and torques experienced by screw-sensed particles are calculated from these 51 resistance tensors, using *slender-filament theory*. The results allow an estimate of the range of buoyancy parameters for which gravitational sedimentation can be neglected. The fundamental component of the particle motion is a rotation, at approximately the same angular velocity as that of the fluid. Superimposed on this are variations, of large period, in the particle orientation. A phase plane analysis is used to find the terminal orientations. Very long calculation times are required for the phase portrait. An approximate method based on azimuthally-averaged equations is developed to avoid the requirements for long time integration.

Key Words: homogeneous shear flow, helical particle, third-rank tensors, separation, particle trajectories

1. INTRODUCTION

The purpose of this paper is to provide a better understanding of the low Reynolds number motion of three-dimensional slender particles in a homogeneous shearing viscous liquid. The particles studied have a specific *dextral* or *sinistral* filament, and have no planes of symmetry.

1.1. Slender-filament theory

Analysis of the Stokes resistance of slender filaments dates back many years (Burgers 1938; Brenner 1966; Batchelor 1970; Tillett 1970; Keller & Rubinow 1976). A very complete formulation was presented by Johnson (1977, 1980), who investigated the families of slender shapes that could be represented by distributing singular solutions of the Stokes equations along the filament centerline. This set of singular solutions is quite extensive, and their functional forms are complex. However, they become considerably simpler in the limit where the filament diameter d becomes small compared to its length $2l$ so that $\epsilon = d/2l$ becomes small.

Under such a formulation, the boundary condition at the particle surface S_p becomes an integral of the singularities along the filament centerline, and the surviving singularities contain only the Stokeslet strength α:

$$\mathbf{V}|_{\text{on } S_p} \to \mathbf{V}_{\mathfrak{C}}(s) = \int_0^{2l} \left[\frac{\boldsymbol{\alpha}(s')}{r} + \frac{\boldsymbol{\alpha} \cdot \mathbf{r}}{r^3} \mathbf{r} \right] \mathrm{d}s'. \qquad [1]$$

Johnson carried out an asymptotic evaluation of this integral for the slender limit.‡ His result displays the leading (logarithmic) contribution coming from the vicinity of the point at which the

‡This limit is referred to in the literature as *slender-body theory*. In the present work, we have adopted the adjective *slender-filament*, to distinguish the slenderness of the filament from that of the body into which the filament is wound, and which need not be slender—see figure 1.

velocity boundary condition is being applied, plus a regular integral over the length of the particle centerline:

$$V_v(s) = \alpha_v(s)L_v + \int_{s_A}^{2l-s_A} K_v[\mathbf{r}_o; \boldsymbol{\alpha}(s')]\,ds', \qquad [2]$$

where the generalized eccentricity is defined by

$$s_A = l[1 - \sqrt{1-\epsilon^2}]$$

and

$$L_t = 2(2L-1), \quad L_b = L_n = 2L+1, \quad L = \ln\frac{2}{\epsilon},$$

and where the integrand K_v, in which v refers to the Frenet triad unit vectors (Struik 1950) $\hat{\mathbf{e}}_t$, $\hat{\mathbf{e}}_b$ and $\hat{\mathbf{e}}_n$ at a field point where the boundary condition is to be satisfied, is defined as

$$K_v[\mathbf{r}_o; \boldsymbol{\alpha}(s')] = \frac{\alpha_v(s')}{r_o} + \frac{[\boldsymbol{\alpha}(s')\cdot\mathbf{r}_o]r_{ov}}{r_o^3} - \frac{D_v\alpha_v(s)}{|s-s'|}, \qquad [3]$$

in which

$$D_t = 2, \quad D_b = D_n = 1.$$

Here s and s' denote the field and source points, and r_o is the distance between them.

1.2. Application to a screw-sensed particle

The geometry of general scew-sensed particles (i.e. corkscrew particle) has the following centerline (figure 1):

$$x = a(s)\cos u, \quad y = ha(s)\sin u, \quad z = bu; \quad 0 \leqslant u \leqslant 2n\pi, \qquad [4]$$

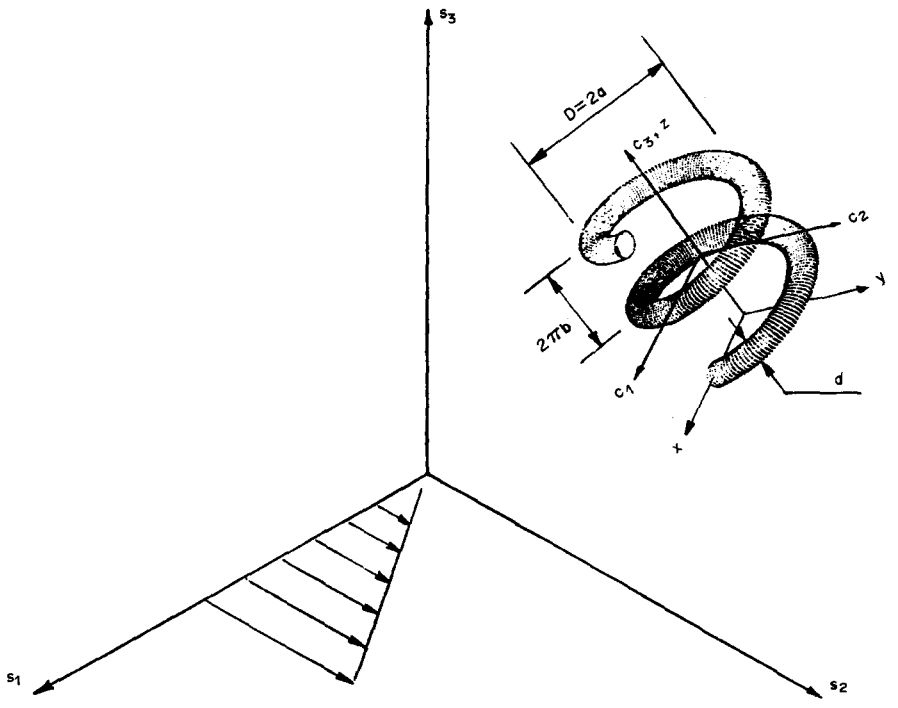

Figure 1. Particle-fixed and space-fixed coordinate systems, and particle geometry.

where $a(s)$ denotes the coil radius at field point s, and $h = 1$ or $h = -1$ for a right- and left-handed particle (RHP and LHP) respectively, and the coil pitch is $2\pi b$. The overall length of coil consisting of n turns (where n need not be an integer) is

$$L = 2\pi nb. \tag{5}$$

The helical particles considered in this paper have constant coil diameter D (radius a) [see also Kim & Rae (1989)] and the components of the position vector $\mathbf{r}_o$ in the kernel K_v can be written as

$$r_{ot} = \frac{a^2}{c}\sin(u-u') + \frac{b^2}{c}(u-u'), \tag{6a}$$

$$r_{ob} = a[\cos(u-u') - 1], \tag{6b}$$

$$r_{on} = h\frac{ab}{c}[(u-u') - \sin(u-u')]; \tag{6c}$$

in which u' denotes the angle at the source point s'.

In addition, with the help of Taylor series expansions, we can derive the special forms of the integrand K_v for the case where the source point coincides with the field point:

$$K_t = -\frac{a}{2c^2}\alpha_b(s), \tag{7a}$$

$$K_b = -\frac{a}{2c^2}\alpha_t(s), \tag{7b}$$

$$K_n = 0. \tag{7c}$$

The force and torque are given by quadratures of the Stokeslet strength as (Chwang & Wu 1974, 1975)

$$\mathbf{F} = -8\pi\mu\int_0^{2l}\boldsymbol{\alpha}\,ds' \tag{8}$$

and

$$\mathbf{T} = -8\pi\mu\int_0^{2l}\mathbf{r}\times\boldsymbol{\alpha}\,ds'. \tag{9}$$

Kim (1987) carried out solutions of [2] following the suggestion made by Brenner (1964) by calculating the force and torque generated for a series of 6 cases, having unit velocity in the directions of each of the 6 degrees-of-freedom. The results of these calculations make it possible to identify all 21 second-rank tensor elements required to examine the complete range of motions of a particle sedimenting under gravity in an unbounded fluid which is otherwise at rest.

We begin the study with the general equations governing the problem for the particle motion, and then show the calculations of hydrodynamic resistance coefficients in section 3. This is followed in section 4 with a study of the special case of slender-needle trajectories, to check the accuracy of our numerical schemes. Following this, motions of screw-shaped particles are examined. A phase plane analysis, including the effects of neutral and nonneutral buoyancy, is used to find the terminal orientations. From these results, we draw some conclusions about the possibility of achieving a resolution of racemic mixtures. However, these results require long integration times. In section 5 an approximate method is developed to minimize the computational time, and section 6 describes the implications of this work on the question of separation. Finally, section 7 contains some remarks about the applicability of this work, and a number of further studies which are now possible.

2. FORMULATION OF EQUATIONS

For the case where the particle is immersed in a constant shear flow, the Stokes problem to be solved is

$$\nabla p = \mu\nabla^2\mathbf{V}, \quad \nabla\cdot\mathbf{V} = 0, \tag{10}$$

with boundary conditions

$$\mathbf{V} = \mathbf{U}_o + \boldsymbol{\omega} \times \mathbf{r}_o \quad \text{on } S_p \tag{11}$$

and

$$\mathbf{V} \to \mathbf{u} = \mathbf{u}_o + \mathbf{r}_o \cdot \mathsf{G} \qquad |\mathbf{r}| \to \infty, \tag{12}$$

where $\mathbf{U}_o$ and $\boldsymbol{\omega}$ denote the particle velocities, $\mathbf{u}_o$ is the undisturbed fluid velocity, $\mathbf{r}_o$ is the position vector of a point relative to an origin at o and G (its magnitude is denoted by G) is the shear dyadic,

$$\mathsf{G} = \nabla \mathbf{u}|_{|\mathbf{r}| \to \infty}, \tag{13}$$

which has the property $\mathsf{I} : \mathsf{G} = 0$, where I is the dyadic idemfactor.

Brenner (1964) has shown that in such a flow the force and torque expressions must include two third-rank tensors that give contributions proportional to the shear rate:

$$\mathbf{F} = -\mu[\mathbf{K} \cdot (\mathbf{U}_o - \mathbf{u}_o) + \mathbf{C}_o^{\dagger} \cdot (\boldsymbol{\omega} - \boldsymbol{\omega}_f) + \boldsymbol{\Gamma}_F : \mathscr{S}] \tag{14}$$

and

$$\mathbf{T}_o = -\mu[\mathbf{C}_o \cdot (\mathbf{U}_o - \mathbf{u}_o) + \boldsymbol{\Omega}_o \cdot (\boldsymbol{\omega} - \boldsymbol{\omega}_j) + \boldsymbol{\Gamma}_T : \mathscr{S}], \tag{15}$$

where: the superscript † denotes the transposition operator; $\boldsymbol{\omega}_j$ is the angular velocity of the fluid spin,

$$\boldsymbol{\omega}_f = \tfrac{1}{2}\nabla \times \mathbf{u}; \tag{16}$$

$\mathscr{S}$, which is symmetric, is the rate of strain dyadic of the undisturbed flow,

$$\mathscr{S} = \tfrac{1}{2}(\mathsf{G} + \mathsf{G}\dagger); \tag{17}$$

and $\mathbf{K}$, $\mathbf{C}_o$, and $\boldsymbol{\Omega}_o$ are second-rank tensors which are called the translational, coupling and rotation tensors, respectively, evaluated at a point o affixed to the particle. The third-rank tensors $\boldsymbol{\Gamma}_F$ and $\boldsymbol{\Gamma}_T$, which are called by Brenner (1964) the *shear-force* and *shear-torque triadics*, are symmetric in their second and third subscripts, and three elements in each tensor can be set to zero in keeping with the incompressibility condition $\mathsf{I} : \mathsf{S} = 0$, which he refers to as the *principle of indeterminacy*. Thus, each of these triadics contains 15 independent coefficients. These resistance tensors depend on the particle shape, and not on the nature of the flow. Some of these will be zero for bodies of certain symmetry classes; Brenner discusses these categories. For a helical coil, all 15 are, in general, nonzero. The numerical values of these dyadics for various helical particle geometries were given by Kim (1987). Here the multiple dot products of polyadics are defined as

$$\begin{aligned} \mathsf{A} : \mathscr{S} &= \sum A_{ijk}\,\mathbf{ijk} : S_{lm}\,\mathbf{lm} \\ &= \sum A_{ijk} S_{lm} \mathbf{i}\underbrace{(\mathbf{k} \cdot \mathbf{l})}_{=\delta_{kl}} \underbrace{(\mathbf{j} \cdot \mathbf{m})}_{=\delta_{jm}}, \end{aligned} \tag{18}$$

where δ_{kl} and δ_{jm} represent the Kronecker delta.

For convenience, the following nondimensionalized variables are introduced:

$$\mathsf{F} = \frac{\mathbf{F}}{\mu a U_{ref}}, \quad \mathsf{T} = \frac{\mathbf{T}}{\mu a^2 U_{ref}}, \quad \mathsf{U} = \frac{\mathbf{U}}{U_{ref}}, \quad \omega = \frac{\omega a}{U_{ref}}, \quad \mathsf{u} = \frac{\mathbf{u}}{U_{ref}}, \quad \omega_f = \frac{\omega_f a}{U_{ref}},$$

$$\mathsf{K} = \frac{\mathbf{K}}{a}, \quad \mathsf{C} = \frac{\mathbf{C}}{a^2}, \quad \Omega = \frac{\boldsymbol{\Omega}}{a^3}, \quad \mathscr{F} = \frac{\boldsymbol{\Gamma}_F}{a^2}, \quad \mathscr{T} = \frac{\boldsymbol{\Gamma}_T}{a^3}, \quad \mathsf{r} = \frac{\mathbf{r}}{a}, \quad \mathsf{S} = \frac{\mathscr{S} a}{U_{ref}}, \quad U_{ref} = \mathrm{Ga}.$$

With the help of the above variables, we have rewritten the hydrodynamic force and torque at the center of mass of particle, which is denoted as $(\,)_c$:

$$\mathsf{F} = -[\mathsf{K} \cdot (\mathsf{U}_c - \mathsf{u}_c) + \mathbf{C}_c^{\dagger} \cdot (\omega_c - \omega_{f,c}) + \mathscr{F}_c : \mathsf{S}] \tag{19}$$

and

$$\mathsf{T}_c = -[\mathsf{C}_c \cdot (\mathsf{U}_c - \mathsf{u}_c) + \Omega_c \cdot (\omega_c - \omega_{f,c}) + \mathscr{T}_c : \mathsf{S}]. \tag{20}$$

3. HYDRODYNAMIC RESISTANCE TENSORS

The motion of a helical particle in a homogeneous shear field can be divided into three sub-problems as follows (Brenner 1964): let the velocity and pressure be expressed as

$$\mathbf{V} = \mathbf{V}_1 + \mathbf{V}_2 + \mathbf{V}_3 \qquad [21]$$

and

$$\mathbf{p} = \mathbf{p}_1 + \mathbf{p}_2 + \mathbf{p}_3, \qquad [22]$$

where all three fields satisfy the Stokes equations, and

	on S_p	$\lvert\mathbf{r}\rvert \to \infty$
$\mathbf{V}_1$	$-\mathscr{S}\cdot\mathbf{r}_o$	0
$\mathbf{V}_2$	$(\mathbf{U}_o - \mathbf{u}_o) + (\boldsymbol{\omega} - \boldsymbol{\omega}_f)\times\mathbf{r}_o$	0
$\mathbf{V}_3$	$\mathbf{u}_o + \boldsymbol{\omega}_f\times\mathbf{r}_o + \mathscr{S}\cdot\mathbf{r}_o$	

Note that the first two sub-problems are variants of the prototype problem solved by Kim (1987), i.e. the determination of the Stokeslet strength for a given velocity distribution along the centerline. The third sub-problem does not contribute to the force or torque on the particle. In addition, the solution of the second sub-problem leads to the **K**, **C** and **Ω** tensors. The surface boundary condition for the first unit problem can be expressed as:

$$V_{1,t} = \frac{a^2}{2c}\sin 2u(\mathscr{S}_{11} - \mathscr{S}_{22}) - h\frac{a^2}{c}\cos 2u\mathscr{S}_{12} + \frac{ab}{c}(u\sin u - \cos u)\mathscr{S}_{13} - h\frac{ab}{c}(u\cos u + \sin u)\mathscr{S}_{23} - \frac{b^2}{c}u\mathscr{S}_{33}, \qquad [23a]$$

$$V_{1,b} = a\cos^2 u\mathscr{S}_{11} + ha\sin 2u\,\mathscr{S}_{12} + bu\cos u\mathscr{S}_{13} + hbu\sin u\mathscr{S}_{23} + a\sin^2 u\mathscr{S}_{22}, \qquad [23b]$$

$$V_{1,n} = -h\frac{ab}{2c}\sin 2u(\mathscr{S}_{11} - \mathscr{S}_{22}) - h\left(\frac{b^2}{c}u\sin u + \frac{a^2}{c}\cos u\right)\mathscr{S}_{13} + \frac{ab}{c}\cos 2u\mathscr{S}_{12} + \left(\frac{b^2}{c}u\cos u - \frac{a^2}{c}\sin u\right)\mathscr{S}_{23} - h\frac{ab}{c}u\mathscr{S}_{33}, \qquad [23c]$$

where $\mathscr{S}_{ij}$ represents the elements of the shear strain dyadic.

All 15 coefficients in the third-rank tensors can be identified by solving the following 6 cases:

Case	S_{11}	S_{22}	S_{33}	S_{12}	S_{13}	S_{23}
7	0	0	0	1	0	0
8	0	0	0	0	1	0
9	0	0	0	0	0	1
10	−1	1	0	0	0	0
11	0	−1	1	0	0	0
12	1	0	−1	0	0	0

The first 3 are based on a homogeneous shear flow (here the unit vectors in space-centered coordinate are denoted by $\hat{\mathbf{s}}_1$, $\hat{\mathbf{s}}_2$ and $\hat{\mathbf{s}}_3$ with the vorticity axis parallel to the direction of gravity). For example, case 8 uses:

$$\mathbf{u} = \mathbf{r}\cdot\hat{\mathbf{s}}_3\hat{\mathbf{s}}_1 = s_3\hat{\mathbf{s}}_1 \qquad [24]$$

and

$$\mathbf{S} = \tfrac{1}{2}(\hat{\mathbf{s}}_1\hat{\mathbf{s}}_3 + \hat{\mathbf{s}}_3\hat{\mathbf{s}}_1), \qquad [25]$$

and the second three are based on the two-dimensional, rectangular hyperbolic shear flow, the so-called *four-roller* flow.

The coefficients identified from each case are (here $\mathscr{A}_{ijk}$ denotes either $\mathscr{F}$ or $\mathscr{T}$ and $\mathscr{B}_i$ denotes either F or T, and the tensor elements $\mathscr{A}_{111}$, $\mathscr{A}_{222}$ and $\mathscr{A}_{333}$ have been taken as zero, using the *principle of indeterminacy*):

$$\text{Case 7:}\quad 2\mathscr{A}_{112} = -\mathscr{B}_1, \quad 2\mathscr{A}_{212} = -\mathscr{B}_2, \quad 2\mathscr{A}_{312} = -\mathscr{B}_3,$$

$$\text{Case 8:}\quad 2\mathscr{A}_{113} = -\mathscr{B}_1, \quad 2\mathscr{A}_{213} = -\mathscr{B}_2, \quad 2\mathscr{A}_{313} = -\mathscr{B}_3,$$

$$\text{Case 9:}\quad 2\mathscr{A}_{123} = -\mathscr{B}_1, \quad 2\mathscr{A}_{223} = -\mathscr{B}_2, \quad 2\mathscr{A}_{323} = -\mathscr{B}_3,$$

$$\text{Case 10:}\quad 2\mathscr{A}_{122} = -\mathscr{B}_1, \quad 2\mathscr{A}_{211} = \mathscr{B}_2,$$

$$\text{Case 11:}\quad 2\mathscr{A}_{133} = \mathscr{B}_1, \quad 2\mathscr{A}_{311} = -\mathscr{B}_3,$$

$$\text{Case 12:}\quad 2\mathscr{A}_{233} = -\mathscr{B}_2, \quad 2\mathscr{A}_{322} = \mathscr{B}_3,.$$

The calculations were done by evaluating the integral equation using an LU-decomposition method with 72 segments per coil pitch on a VAX 8650 (Brown 1990).

The transformation laws for the *shear-force* and *shear-torque triadics* at an arbitrary point p are given by Brenner (1964):

$$\mathscr{F}_p = \mathscr{F}_o + \tfrac{1}{2}[\mathsf{K}r_{op} + (\mathsf{K}r_{op})\dagger] \qquad [26]$$

and

$$\mathscr{T}_p = \mathscr{T}_o + \tfrac{1}{2}[\mathsf{C}_p r_{op} + (\mathsf{C}_p r_{op})\dagger] - r_{op} \times \mathscr{F}_o, \qquad [27]$$

in which r_{op} is the distance from the origin to an arbitrary point p.

Numerical results for *shear-force* and *shear-torque triadics* for helical particles having the geometry $L/D = 1$, $n = 2$ and $d/2a = 0.1$ are given in table 1 along with values of the second-rank tensors. The magnitudes of the shear tensor elements, $\mathscr{F}_{c111,(122,123,213,312,313)}$, $\mathscr{T}_{c122,(123,212,213,313)}$, referred to the center of mass, are about 10 times larger than the others. We have plotted these third-rank resistance tensors for various particle geometries in figures 2 and 3. All the elements of the third-rank

Table 1. Comparison of resistance tensors between helical RHP and LHP for $L/D = 1$, $n = 2$, $d/2a = 0.1$

Tensors	RHP			LHP		
K_{ij}	1.764E+01	5.023E−04	8.167E−04	1.764E+01	−5.023E−04	8.167E−04
	5.023E−04	1.775E+01	5.368E−01	−5.023E−04	1.775E+01	−5.368E−01
	8.167E−04	5.368E−01	1.938E+01	8.167E−04	−5.368E−01	1.938E+01
$\mathsf{C}_{c,ij}$	6.970E−01	−1.060E−02	−1.123E−03	−6.970E−01	−1.060E−02	1.123E−03
	1.731E−03	−3.233E−02	2.264E−01	1.731E−03	3.233E−02	2.264E−01
	4.101E−03	−1.749E−01	−6.656E−01	−4.101E−03	−1.749E−01	6.656E−01
$\Omega_{c,ij}$	2.955E+01	1.627E−03	−2.057E−02	2.955E+01	−1.627E−03	−2.057E−02
	1.627E−03	2.942E+01	2.581E+00	−1.627E−03	2.942E+01	−2.581E+00
	−2.057E−02	2.581E+00	2.690E+01	−2.057E−02	−2.581E+00	2.690E+01
$\mathscr{F}_{c,ijk}$	2.053E−01	3.339E−04	6.002E−03	2.053E−01	−3.339E−04	6.002E−03
	3.339E−04	−1.244E−01	−2.321E−01	−3.339E−04	−1.244E−01	2.321E−01
	6.002E−03	−2.321E−01	−8.097E−02	6.002E−03	2.321E−01	−8.097E−02
	−2.753E−04	9.856E−02	2.959E−01	2.753E−04	9.856E−02	−2.959E−01
	9.856E−02	−1.350E−03	−1.115E−04	9.856E−02	1.350E−03	−1.115E−04
	2.959E−01	−1.115E−04	1.625E−03	−2.959E−01	−1.115E−04	−1.625E−03
	3.772E−03	−2.188E−01	3.124E−01	3.772E−03	2.188E−01	3.124E−01
	−2.188E−01	4.381E−03	−2.084E−03	2.188E−01	4.381E−03	2.084E−03
	3.124E−01	−2.084E−03	−8.153E−03	3.124E−01	2.084E−03	−8.153E−03
$\mathscr{T}_{c,ijk}$	−5.910E−01	2.851E−03	4.577E−03	5.910E−01	2.851E−03	−4.577E−03
	2.851E−03	−4.682E+00	−3.605E+00	2.851E−03	4.682E+00	−3.605E+00
	4.577E−03	−3.605E+00	5.273E+00	−4.577E−03	−3.605E+00	−5.273E+00
	−8.791E−04	2.461E+00	3.652E+00	−8.791E−04	−2.461E+00	3.652E+00
	2.461E+00	−5.931E−03	3.637E−03	−2.461E+00	−5.931E−03	−3.637E−03
	3.652E+00	3.637E−03	6.810E−03	3.652E+00	−3.637E−03	6.810E−03
	3.795E−02	−5.275E−02	−1.794E+00	−3.795E−02	−5.275E+00	1.794E+00
	−5.275E−02	3.844E−02	−2.056E−02	−5.275E−02	−3.844E−02	−2.056E−02
	−1.794E+00	−2.056E−02	−7.640E−02	1.794E+00	−2.056E−02	7.640E−02

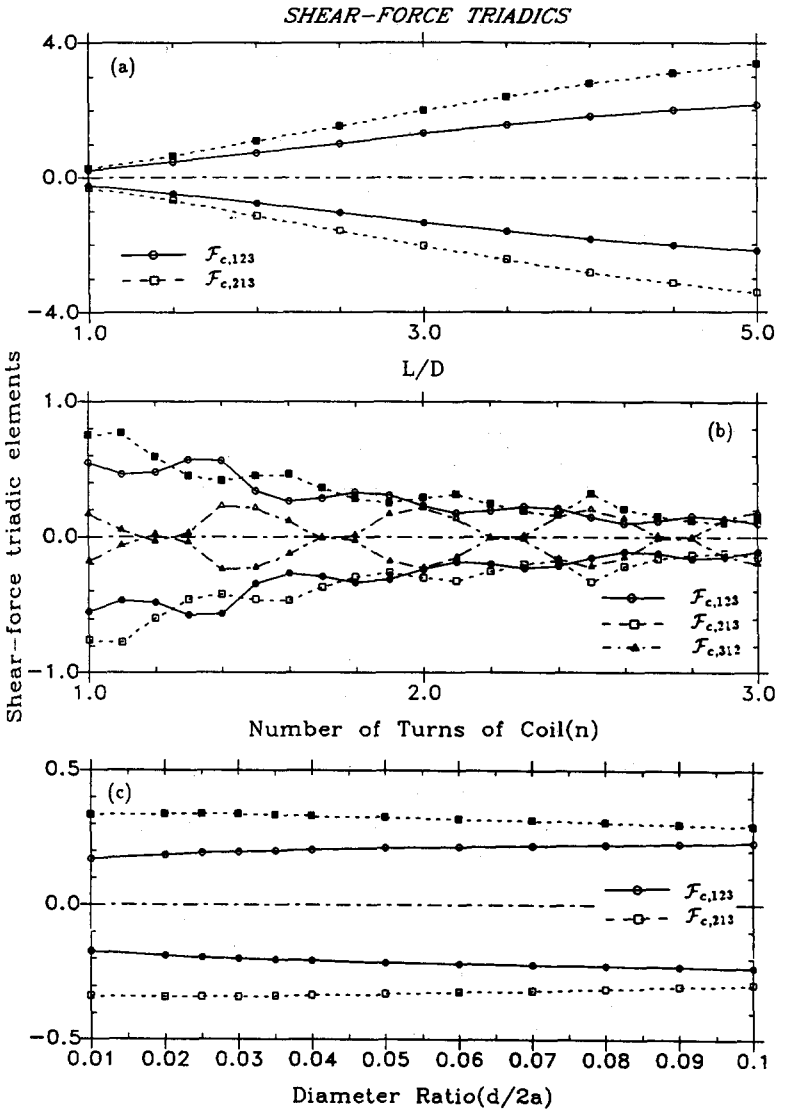

Figure 2. Variation of the *shear-force triadic* elements with respect to three geometrical conditions: (a) L/D; (b) n; and (c) $d/2a$. The basic particle geometry is $L/D = 1$, $n = 2$ and $d/2a = 0.1$; solid symbols—RHP, open symbols—LHP.

tensors vary monotonically with L/D, and $d/2a$, but not for variations with the number of turns of the coil.

With the knowledge of these 51 scalar resistance coefficients, i.e. 6 for the translation tensor, 9 for the coupling tensor, 6 for the rotation tensor and 15 elements for each of the *shear-force* and *shear-torque triadics*, the hydrodynamic force and torque on rigid particles undergoing given translational and rotational motions in a homogeneous shear flow are completely defined.

Examination of table 1 shows that certain elements of the resistance tensors are, numerically, quite small. Some of these small terms might be exactly zero, raising the question whether the retention of small but nonzero effects over a long time-integration period may lead to erroneous results when predicting the particle motion.‡ We will discuss these effects in section 4.

To check the accuracy of the numerical schemes being used here, we compare the resistance tensors for a straight rigid ellipsoidal particle with the analytical formulas (Brenner 1964). Due to the symmetry of an ellipsoidal particle, the coupling tensor and *shear-force triadic* are zero. Also, the slender-needle geometry can be approximated as a helical coil having a vanishing number of turns.

‡The referees have suggested that it might be possible to show by symmetry arguments that some of these coefficients are identically zero; to date, we have been unable to provide such a proof.

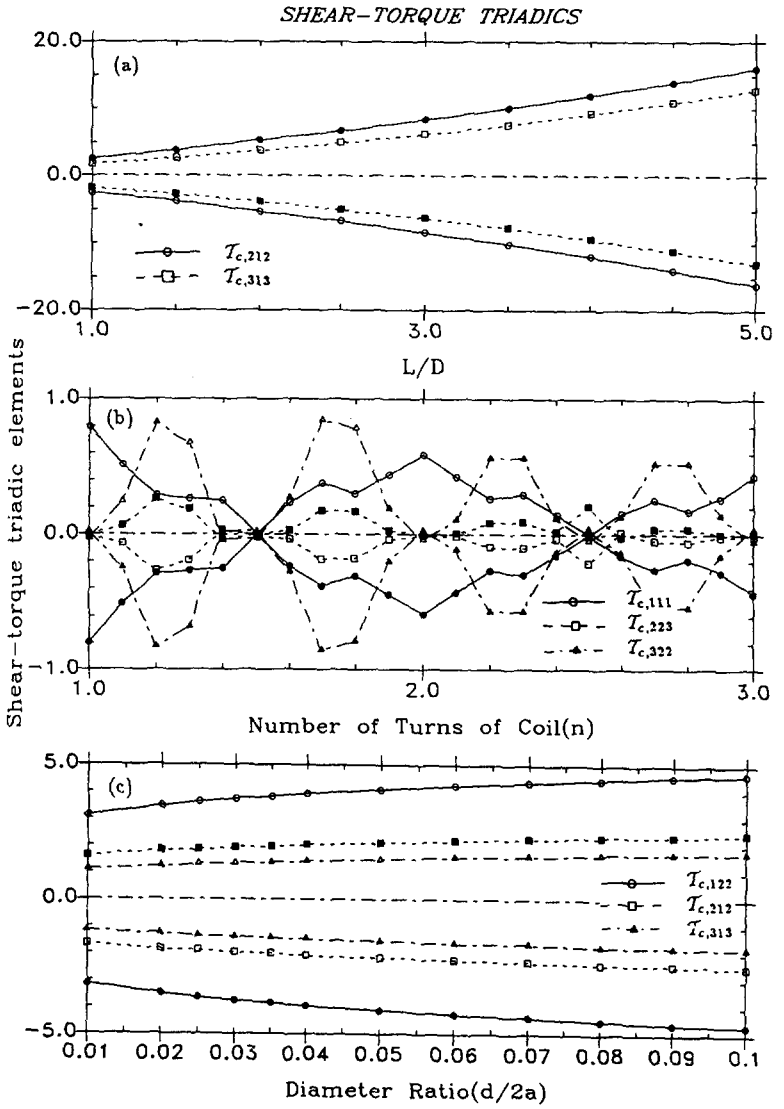

Figure 3. Variation of the *shear-torque triadic* elements with respect to three geometrical conditions: (a) L/D; (b) n; and (c) $d/2a$. The basic particle geometry is $L/D = 1$, $n = 2$ and $d/2 = 0.1$; solid symbols—RHP, open symbols—LHP.

Table 2 shows a comparison of the numerical values of tensors for a slender needle whose equatorial diameter is one-hundredth of its length, which we have represented as a helical particle having the geometry $L/D = 1, n = 0.0001$ and $d/2a = 0.01$. These results show excellent agreement with the analytical formulas.

In a following section, we shall show the analysis of the particle motions in a constant shear field using the above hydrodynamic resistance tensors.

4. TRAJECTORIES

4.1. *Equations of motion*

At low Reynolds number conditions, it is possible to neglect all particle acceleration terms after a short time of order $m_p/\mu a$, where m_p is the mass of the particle.‡ The resulting equations, which we have called the *quasi-terminal* equations (Kim & Rae 1989) are:

‡We are grateful to Professors C. P. Yu and J. D. Felske for pointing out to us that for particles of neutral buoyancy, it may be necessary to include here the effects of *apparent mass* and the viscous-history forces described by the *Bassett* integral.

Table 2. Comparison of resistance tensors for a slender needle between analytical formulas and *slender-filament theory*

Tensors	Brenner (1964)			Slender-filament theory		
K_{ij}	4.334	0	0	4.334E+00	8.025E−11	1.692E−07
	0	4.334	0	8.025E−11	4.334E+00	−5.389E−04
	0	0	2.619	1.692E−07	−5.389E−04	2.619E+00
$C_{c,ij}$		0		−8.389E−11	4.768E−07	7.743E−05
				−9.537E−07	2.910E−10	2.384E−07
				−1.282E−04	9.537E−07	0.000E+00
$\Omega_{c,ij}$	1.746	0	0	1.747E+00	3.492E−10	9.537E−07
	0	1.746	0	4.657E−10	1.747E+00	−5.487E−04
	0	0	0.001	9.537E−07	−5.487E−04	−4.768E−07
$\mathscr{F}_{c,ijk}$		0		−9.537E−07	−6.408E−05	−2.384E−07
				−6.408E−05	4.768E−07	−8.958E−11
				−2.384E−07	−8.958E−11	−9.537E−07
				4.272E−05	−2.384E−07	2.619E−10
				−2.384E−07	−8.544E−05	2.384E−07
				2.619E−10	2.384E−07	4.272E−05
				−7.153E−07	5.821E−11	1.192E−07
				5.821E−11	−2.384E−07	−3.872E−05
				1.192E−07	−3.872E−05	7.153E−07
$\mathscr{T}_{c,ijk}$	0	0	0	5.821E−11	−7.153E−07	−5.821E−11
	0	0	0.872	−7.153E−07	5.487E−04	8.733E−01
	0	0.872	0	−5.821E−11	8.733E−01	−5.487E−04
	0	0	−0.872	5.960E−07	−2.744E−04	−8.733E−01
	0	0	0	−2.744E−04	−8.345E−07	8.731E−11
	−0.872	0	0	−8.733E−01	8.731E−11	−5.960E−07
		0		−4.075E−10	4.768E−07	2.744E−04
				4.768E−07	5.239E−10	7.153E−07
				2.744E−04	7.153E−07	5.821E−11

$$\mathsf{F} = \mathsf{Y}\hat{\mathsf{s}}_3 \tag{28}$$

and

$$\mathsf{T}_c = 0, \tag{29}$$

where the buoyancy parameter Y, is proportional to the ratio of the terminal velocity due to gravitational settling to the characteristic shear flow velocity

$$\mathsf{Y} \sim \frac{(m_p - m_f)g}{\mu G a^2}; \tag{30}$$

in which m_f denotes the mass of the fluid displaced by the particle.

From [28] and [29], the formulas of the angular and linear velocities of the particle can be deduced as:

$$\omega_c = \omega_{f,c} + \mathbf{B}_c \cdot \mathsf{Y}\hat{\mathsf{s}}_3 + \mathbf{P}_c : \mathsf{S} \tag{31}$$

and

$$\mathsf{U}_c = \mathsf{u}_c + \mathbf{R}_c \cdot \mathsf{Y}\hat{\mathsf{s}}_3 + \mathbf{Q}_c : \mathsf{S}, \tag{32}$$

where the second-rank tensors $\mathbf{B}_c$ and $\mathbf{R}_c$, and third-rank tensors $\mathbf{P}_c$ and $\mathbf{Q}_c$ are defined as:

$$\mathbf{B}_c = [\mathsf{K} \cdot \mathsf{C}_c^{-1} \cdot \boldsymbol{\Omega}_c - \mathsf{C}_c^{\dagger}]^{-1} \tag{33}$$

and

$$\mathbf{R}_c = -\mathsf{C}_c^{-1} \cdot \boldsymbol{\Omega}_c \cdot \mathbf{B}_c; \tag{34}$$

and

$$\mathbf{P}_c = B_c \cdot (\mathscr{F}_c - \mathsf{K} \cdot \mathsf{C}_c^{-1} \cdot \mathscr{T}_c) \tag{35}$$

and

$$\mathbf{Q}_c = [\mathsf{C}_c^{\dagger} \cdot \boldsymbol{\Omega}_c^{-1} \cdot \mathsf{C}_c - \mathsf{K}]^{-1} \cdot (\mathscr{F}_c - \mathsf{C}_c^{-1} \cdot \boldsymbol{\Omega}_c^{-1} \cdot \mathscr{T}_c). \tag{36}$$

As Kim (1990) has shown, the elements of dyadics $\mathbf{B}_c$ and $\mathbf{R}_c$ for both right- and left-handed particles have the same sign symmetries as the coupling and translational (or rotational) tensors, respectively. In addition, the elements of triadics $\mathbf{P}_c$ and $\mathbf{Q}_c$ are symmetric in their second and third indices. For RHP and LHP the elements of these third-rank tensors have the same sign symmetries as the *shear-torque triadic* and *shear-force triadic*, respectively.

In order to define the orientation of a particle, we require the transformation between two sets of coordinates (figure 4), one of which is particle-fixed (c_1, c_2, c_3) with origin at the center of mass with unit vectors $\hat{\mathbf{c}}_1, \hat{\mathbf{c}}_2$ and $\hat{\mathbf{c}}_3$, and the other space-fixed (s_1, s_2, s_3) with unit vectors of $\hat{\mathbf{s}}_1$ $\hat{\mathbf{s}}_2$ and $\hat{\mathbf{s}}_3$. The coordinate transformation can be expressed as a function of the Euler angles (Goldstein 1980), i.e. azimuthal(ϕ), polar(θ) and roll(ψ) angles (see figure 4):

$$\begin{Bmatrix} \hat{\mathbf{c}}_1 \\ \hat{\mathbf{c}}_2 \\ \hat{\mathbf{c}}_3 \end{Bmatrix} = [m_{ij}] \begin{Bmatrix} \hat{\mathbf{s}}_1 \\ \hat{\mathbf{s}}_2 \\ \hat{\mathbf{s}}_3 \end{Bmatrix}, \tag{37}$$

where the matrix $[m_{ij}]$ (whose inverse is equal to its transpose) is:

$$\left.\begin{aligned} m_{11} &= \cos\phi\cos\psi - \sin\phi\cos\theta\sin\psi, \\ m_{12} &= \sin\phi\cos\psi + \cos\phi\cos\theta\sin\psi, \\ m_{13} &= \sin\theta\sin\psi, \\ m_{21} &= -\cos\phi\sin\psi - \sin\phi\cos\theta\cos\psi, \\ m_{22} &= -\sin\phi\sin\psi + \cos\phi\cos\theta\cos\psi, \\ m_{23} &= \sin\theta\cos\psi, \\ m_{31} &= \sin\phi\sin\theta, \\ m_{32} &= -\cos\phi\sin\theta. \\ m_{33} &= \cos\theta. \end{aligned}\right\} \tag{38}$$

Furthermore, the rates of change of the Euler angles are:

$$\frac{d\phi}{d\tau} = \frac{1}{\sin\theta}(\sin\psi\,\omega_{c_1} + \cos\psi\omega_{c_2}), \tag{39a}$$

$$\frac{d\theta}{d\tau} = \cos\psi\,\omega_{c_1} - \sin\psi\omega_{c_2}, \tag{39b}$$

$$\frac{d\psi}{d\tau} = \omega_{c_3} - \frac{\cos\theta}{\sin\theta}(\sin\psi\,\omega_{c_1} + \cos\psi\omega_{c_2}); \tag{39c}$$

in which τ represents the dimensionless time defined by

$$\tau = Gt. \tag{40}$$

In a constant shear flow field (figure 1), in which the planes of shear are parallel to the s_3-axis and the linear velocity U_{s_2} is parallel to the streamlines, the shear strain dyadic of the undistributed flow is:

$$\begin{aligned} \mathsf{S} &= \frac{1}{2}(\hat{\mathbf{s}}_1\hat{\mathbf{s}}_2 + \hat{\mathbf{s}}_2\hat{\mathbf{s}}_1) \\ &= \frac{1}{2}\begin{bmatrix} D_{11}\hat{\mathbf{c}}_1\hat{\mathbf{c}}_1 + D_{12}\hat{\mathbf{c}}_1\hat{\mathbf{c}}_2 + D_{13}\hat{\mathbf{c}}_1\hat{\mathbf{c}}_3 \\ + D_{21}\hat{\mathbf{c}}_2\hat{\mathbf{c}}_1 + D_{22}\hat{\mathbf{c}}_2\hat{\mathbf{c}}_2 + D_{23}\hat{\mathbf{c}}_2\hat{\mathbf{c}}_3 \\ + D_{31}\hat{\mathbf{c}}_3\hat{\mathbf{c}}_1 + D_{32}\hat{\mathbf{c}}_3\hat{\mathbf{c}}_2 + D_{33}\hat{\mathbf{c}}_3\hat{\mathbf{c}}_3 \end{bmatrix}, \end{aligned} \tag{41}$$

where the D_{ij}-elements can be written in a form that displays the entire azimuthal angle dependence:

$$D_{ij} = DS_{ij}\sin 2\phi + DC_{ij}\cos 2\phi. \tag{42}$$

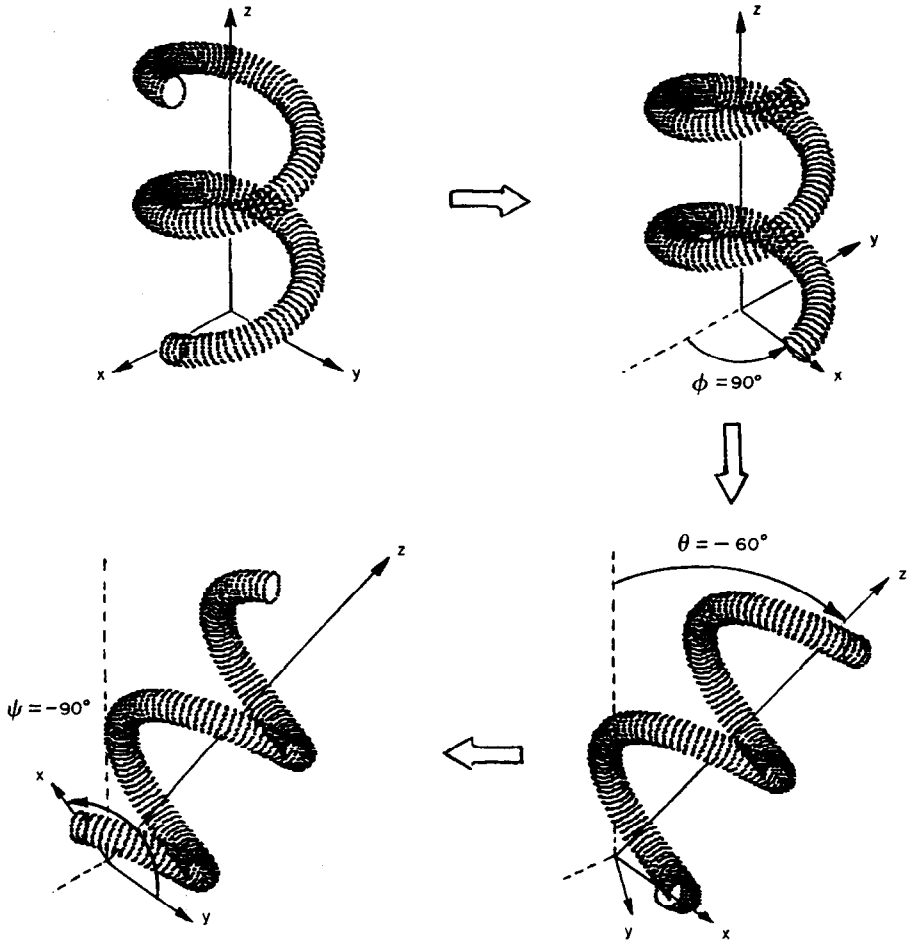

Figure 4. Configuration of the Euler angles of a right-handed helix.

Here the elements DS_{ij} and DC_{ij} depend only on θ and ψ, and are defined as:

$$DS_{ij} = \begin{Bmatrix} \cos^2\psi - \cos^2\theta \sin^2\psi & -\frac{1}{2}(1+\cos^2\theta)\sin 2\psi & \frac{1}{2}\sin 2\theta \sin\psi \\ -\frac{1}{2}(1+\cos^2\theta)\sin 2\psi & \sin^2\psi - \cos^2\theta\cos^2\psi & \frac{1}{2}\sin 2\theta\cos\psi \\ \frac{1}{2}\sin 2\theta\sin\psi & \frac{1}{2}\sin 2\theta\cos\psi & -\sin^2\theta \end{Bmatrix} \quad [43]$$

and

$$DC_{ij} = \begin{Bmatrix} \cos\theta\sin 2\psi & \cos\theta\cos 2\psi & -\sin\theta\cos\psi \\ \cos\theta\cos 2\psi & -\cos\theta\sin 2\psi & \sin\theta\sin\psi \\ -\sin\theta\cos\psi & \sin\theta\sin\psi & 0 \end{Bmatrix}. \quad [44]$$

For easier analysis, we can express the last terms of [31] and [32] as follows, where Γ_{ijk} denotes either the elements of $\mathscr{P}_{c,ijk}$ or $\mathscr{Q}_{c,ijk}$:

$$(\Gamma : \mathrm{S})_{i(i=1,2,3)} = \tfrac{1}{2}(GS_i \sin 2\phi + GC_i \cos 2\phi), \quad [45]$$

where

$$GS_i = \Gamma_{i11}DS_{11} + \Gamma_{i22}DS_{22} + \Gamma_{i33}DS_{33} + 2(\Gamma_{i12}DS_{12} + \Gamma_{i13}DS_{13} + \Gamma_{i23}DS_{23}) \quad [46]$$

and

$$GC_i = \Gamma_{i11}DC_{11} + \Gamma_{i22}DC_{22} + \Gamma_{i33}DC_{33} + 2(\Gamma_{i12}DC_{12} + \Gamma_{i13}DC_{13} + \Gamma_{i23}DC_{23}). \quad [47]$$

Finally, the location of the center of mass in the space-fixed coordinates is found from

$$\frac{ds_i}{d\tau} = U_{c,m,i}, \qquad [48]$$

where s_i and $U_{c,m,i}$ denote the nondimensionalized location of the center of mass in space-fixed coordinates, and the translational velocity. In this paper, we have used a fourth-order Runge–Kutta scheme to find the orientation and location of the particles.

4.2. *Trajectories and phase plane diagram*

As a check on our methods of integrating the 6 degrees-of-freedom motions, we calculated the motion of a rigid ellipsoid of revolution. A comparison of our results with the analytic solution of Jeffrey is given in Kim (1990); the comparison is excellent, and leads us to conclude that our numerical methods are accurate.

We now consider a screw-sensed particle having constant coil radius a and having the geometry $L/D = 1$, $n = 2$ and $d/2a = 0.1$. First, the trajectories of a neutrally-buoyant particle are plotted in figures 5 and 6 with $\phi_o/\theta_o/\psi_o = 0°/-90°/-90°$. The Euler-angle histories show two different

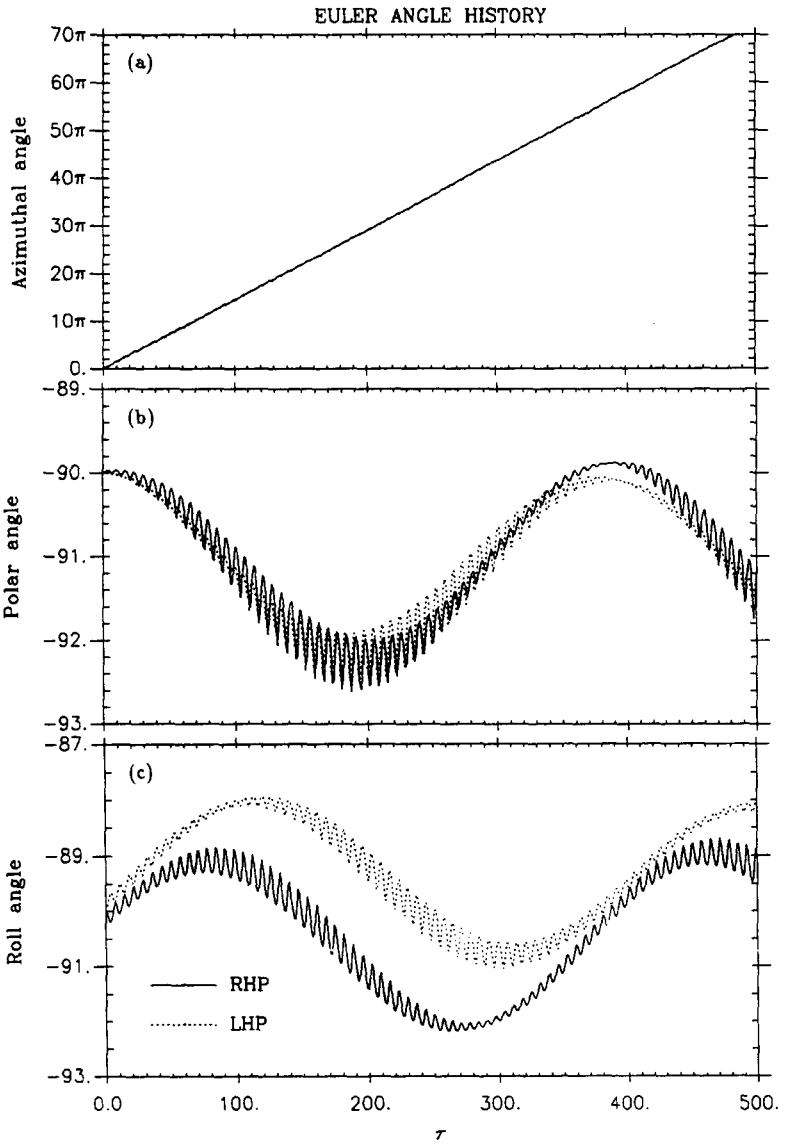

Figure 5. Euler-angle histories of neutrally-buoyant RHP and LHP with an initial condition $\phi_o/\theta_o/\psi_o = 0°/-90°/-90°$.

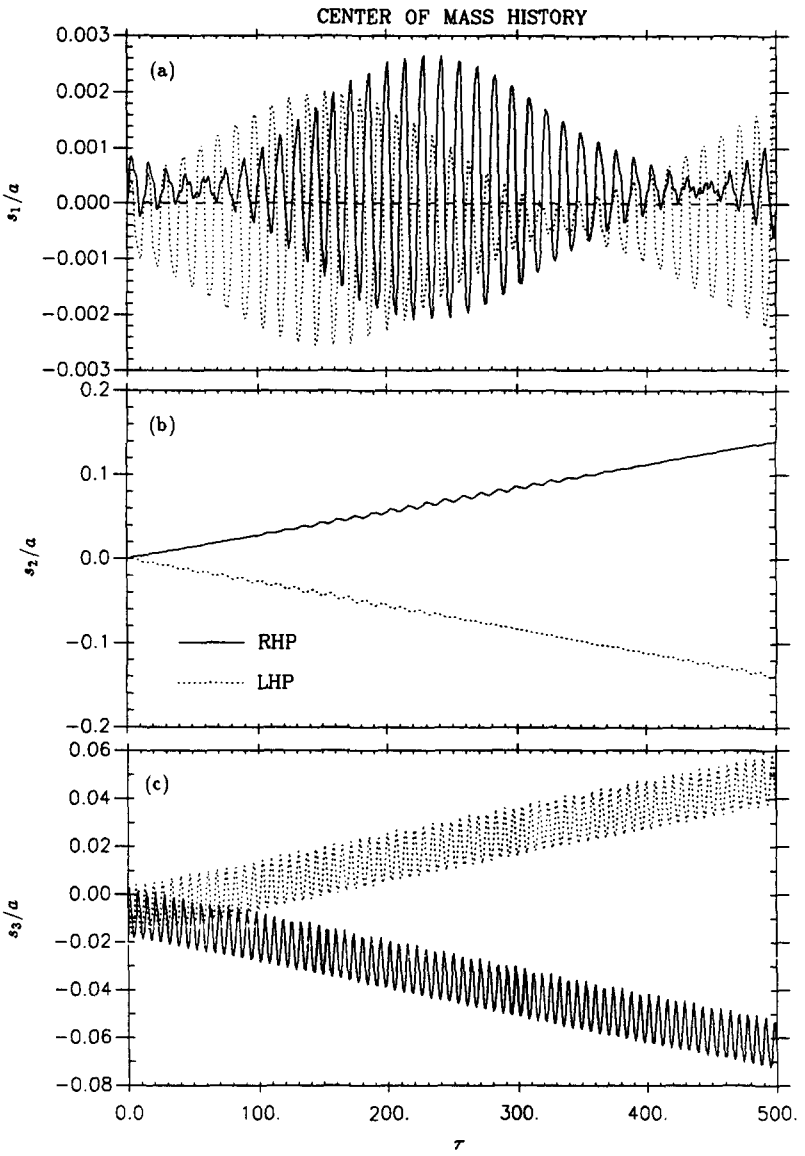

Figure 6. Center-of-mass histories of neutrally-buoyant RHP and LHP with an initial condition $\phi_o/\theta_o/\psi_o = 0°/-90°/-90°$.

periods; one a short-period oscillation (here called the *primary oscillation*) whose period is proportional to $2\pi/G$; the other a long-period oscillation (*secondary oscillation*) with small deviations from the initial values (except for the azimuthal angle which for both RHP and LHP increases linearly, with a small sinusoidal oscillation superimposed on the linear growth).

Figure 6(b) shows a steady migration of neutrally-buoyant RHP and LHP along the positive s_2-direction due to the fact that its average s_1-location is nonzero. The slope $\dot{s}_2$ is essentially equal to the mean nonzero value of s_1. The particles oscillate about a steady drift in the negative s_3-direction.

Figures 7–10 show the histories of nonneutrally-buoyant particles with the initial condition $\phi_o\,\theta_o\psi_o = 0°/-90°/-90°$ for various values of Y. As with a neutrally-buoyant particle, the azimuthal angle histories for both screw senses show linear variations with τ even at the higher Y-value shown. However, the polar angle shows small deviations from the initial θ_o-value, except for $Y = 10$. This phenomenon can be explained by introducing a phase plane analysis, i.e. we show a plot of θ vs ψ for $Y = 1$ and $Y = 100$ in figures 11 and 12. These phase portraits show several critical zones; for an RHP; an unstable zone, $\theta/\psi \approx -90°/-90°$; a stable zone, $-270°/-90°$ and a saddle zone, for $Y = 1$, $-110°/-180°$, for $Y = 100$, $-102°/-180°$. We here use the term *zone* instead of *foci* or *point* because the ϕ variation spreads the motion over a narrow region.

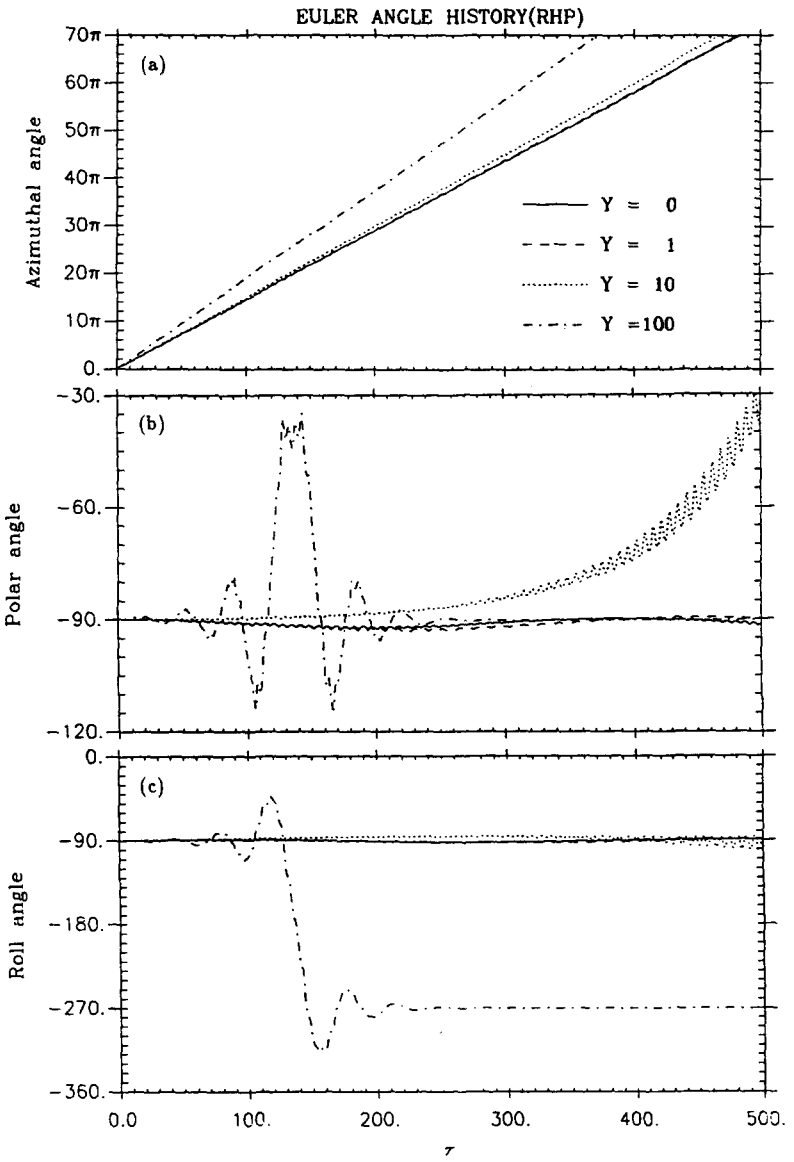

Figure 7. Euler-angle histories of nonneutrally-buoyant RHP with various buoyancy parameters for $\phi_o/\theta_o/\psi_o = 0°/-90°/-90°$.

We may conclude that $Y \approx 10$ is intermediate between shear-dominated ($Y \to 0$) and gravitational-settling dominated ($Y \to \infty$) values. The roll-angle histories show the same properties as do the polar angles, except for the case $Y = 100$, where for both particles, ψ converges to $-270°$.

It is clear from these phase portraits that for each particle and each value of Y there are one or more zones that may be terminal orientations. For the strictly two-dimensional phase planes discussed in Kim (1987) and Kim & Rae (1989), every point in the plane was connected to one unique terminal point by the trajectory passing through it. For the present case, no such unique relations can be stated: most of the orientation space appears connected to only one of the terminal zones, but there are areas—particularly near the saddle zones—where it is difficult to predict which terminal orientation will result.

These features of the motion might be symptomatic of chaotic behavior, i.e. the question arises whether particles starting near the saddle zones display a fractal interweaving of their terminal orientations. We made a limited search for this behavior, by examining a series of trajectories starting from the vicinity of the region $\theta/\psi = -70°/0°$ for an RHP having $Y = 100$. No evidence of chaotic behavior was found, and the question has not been pursued further.

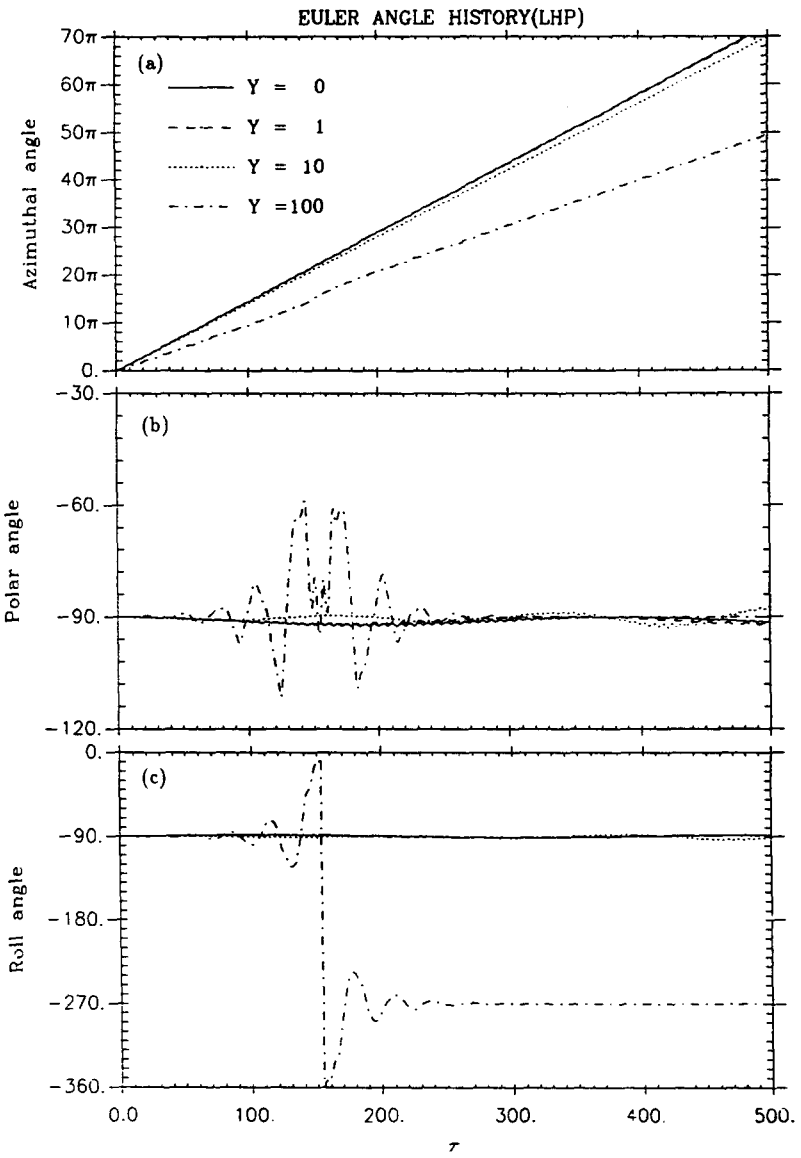

Figure 8. Euler-angle histories of nonneutrally-buoyant LHP with various buoyancy parameters for $\phi_o/\theta_o/\psi_o = 0°/-90°/-90°$.

As mentioned earlier, the effects of retaining small nonzero tensor values may lead to erroneous results over a long time-integration, especially in cases where the particle migration is already quite small. In an attempt to resolve this question, we made a series of runs in which we set equal to zero all tensor elements which were in absolute value 10^{-3} times smaller than the largest element of that tensor. The results were qualitatively similar to those found when retaining the small tensor elements, i.e. the terminal orientations and the general motion characteristics noted above were unchanged.

We can interpret the results for large Y-values by considering the motion to consist principally of sedimentation, perturbed by a small shear. For pure sedimentation, particles of opposite screw sense will achieve terminal states in which the values of $\dot{s}_3$ are identical, but the value of ω_{s_3} are opposite. For gravitational settling, the value of ω_{s_3}, taken from Kim (1987), is

$$\begin{aligned}\omega_{s_3}|_{\text{grav}} = {} & \sin^2\theta \sin^2\psi \mathbf{B}_{c,11} + \sin^2\theta \sin\psi \cos\psi (\mathbf{B}_{c,12} + \mathbf{B}_{c,21}) \\ & + \sin^2\theta \cos^2\psi \mathbf{B}_{c,22} + \sin\theta \cos\theta \cos\psi (\mathbf{B}_{c,23} + \mathbf{B}_{c,32}) \\ & + \cos^2\theta \mathbf{B}_{c,33} + \sin\theta \cos\theta \sin\psi (\mathbf{B}_{c,13} + \mathbf{B}_{c,31}),\end{aligned} \quad [49]$$

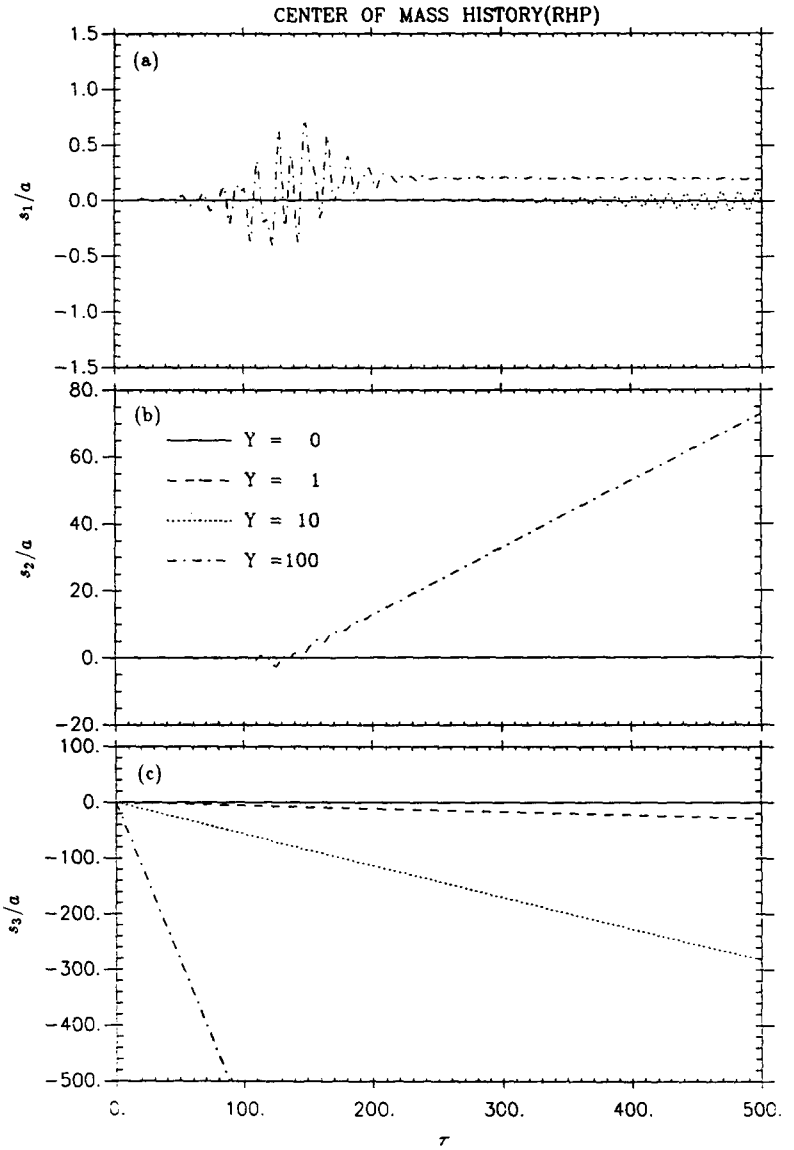

Figure 9. Center-of-mass histories of nonneutrally-buoyant RHP with various buoyancy parameters for $\phi_o/\theta_o/\psi_o = 0°/-90°/-90°$.

which can be written as $f(\mathbf{B}_c)$ since θ and ψ take their terminal values, which also depend only on the $\mathbf{B}_c$-matrix.

In a constant shear flow field, the angular velocity reached at large time is

$$\omega_{s_3}|_{\text{shear}} = 0.5 + f(\mathbf{B}_c)\mathrm{Y} + g(\mathbf{P}_c; \phi, \theta, \psi), \tag{50}$$

where

$$g(\mathbf{P}_c; \phi, \theta, \psi) = \frac{1}{2}\sum_{i=1}^{3} m_{i3}\left\{\begin{array}{l} \mathscr{P}_{ci11} D_{11} + \mathscr{P}_{c,i22} D_{22} + \mathscr{P}_{c,i33} D_{33} \\ +2(\mathscr{P}_{c,i12} D_{12} + \mathscr{P}_{c,i13} D_{13} + \mathscr{P}_{c,i23} D_{23}) \end{array}\right\}. \tag{51}$$

The terminal state shown in figure 12 is $\theta/\psi = -90°/-270°$ for particles of either screw sense. This is also the terminal orientation favored for most initial orientations for the no-shear case. For this terminal orientation, only the $\mathbf{B}_{c,11}$ element enters the final formula, and it is antisymmetric in h:

$$\omega_{s_3} = 0.5 \pm |\mathbf{B}_{c,11}|\mathrm{Y} + O(\mathbf{P}_c). \tag{52}$$

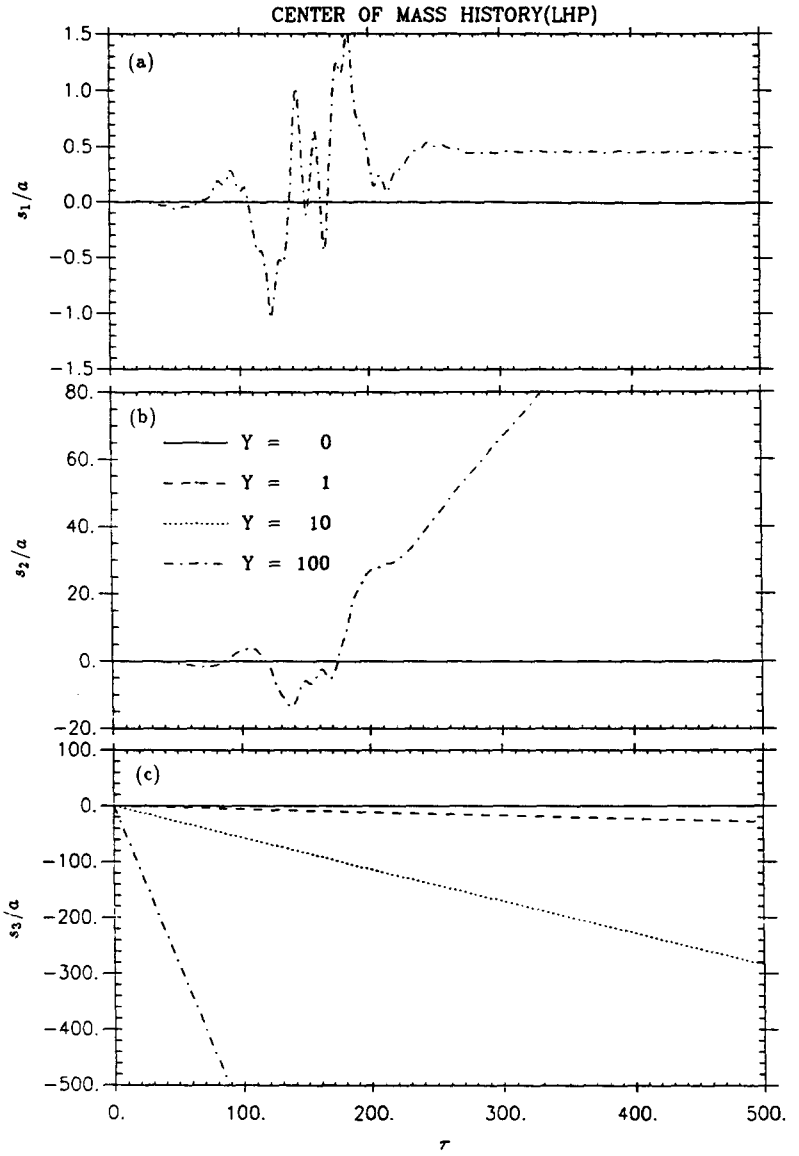

Figure 10. Center-of-mass histories of nonneutrally-buoyant LHP with various buoyancy parameters for $\phi_o/\theta_o/\psi_o = 0°/-90°/-90°$.

The physical interpretation of this result is that the particle's angular velocity is composed of the fluid spin plus or minus the gravity-induced rotation, and modulated by a relatively small fluctuation arising from the $\mathbf{P}_c$ terms. Because the element $\mathbf{B}_{c,11}$ has the value $\pm 1.338 \times 10^{-3}$, it is clear that ω_{s_3} will be zero for the value

$$\mathrm{Y} = -\frac{0.5 + g(\mathbf{P}_c; \phi, \theta, \psi)}{|\mathbf{B}_{c,11}|}$$

$$= 374 + O(\mathbf{P}_c), \qquad [53]$$

i.e. an LHP will ultimately sink without rotation for this value of Y, while an RHP will rotate with roughly twice the fluid spin. The occurrence of this phenomenon is the explanation for some of the apparently anomalous behavior seen in figures 7 and 8, where the curves for Y = 100 were beginning to approach this threshold.

It should be noted that for even large Y-values (>700, say)) the terminal spin is dictated solely by gravity, with that due to fluid spin being a small correction.

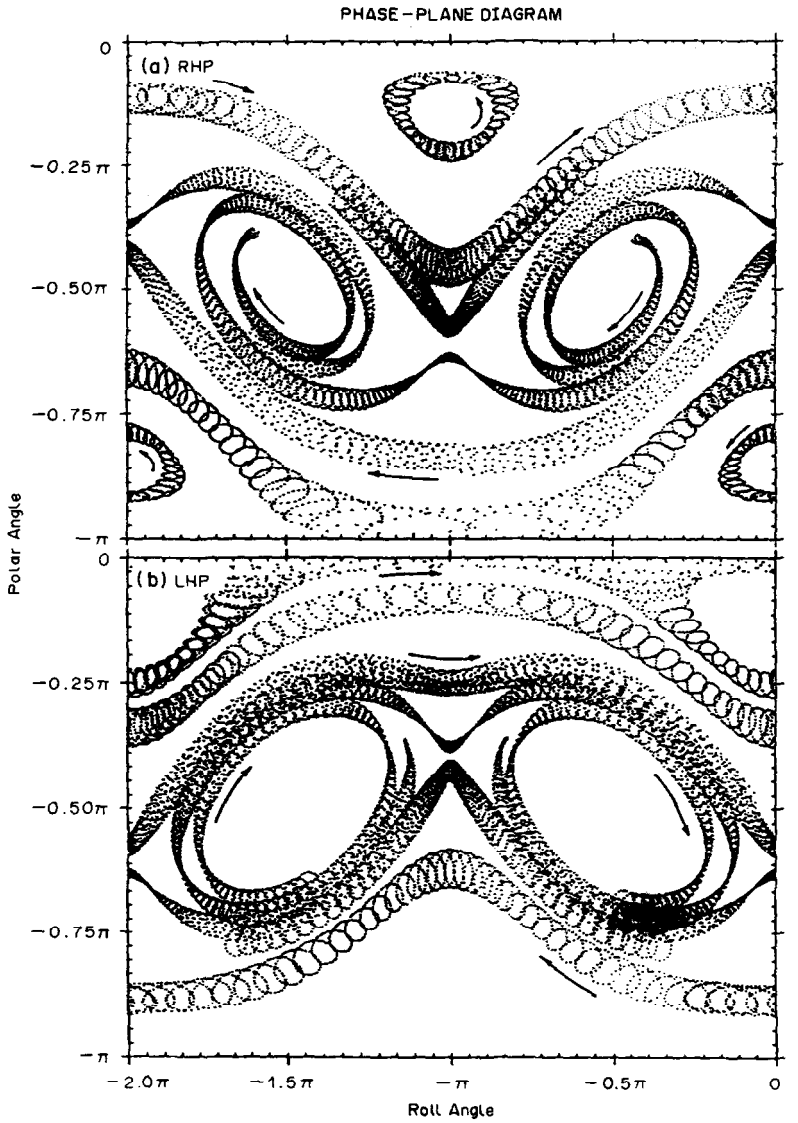

Figure 11. Phase-plane diagram of helical particles for $L/D = 1$, $n = 2$, $d/2a = 0.1$ and $Y = 1$.

5. APPROXIMATE METHOD

A limitation of the previous phase-plane analysis is the long computational time required to find the terminal orientation of the particles. In particular, the period of the azimuthal motion for a small buoyancy parameter is very long. However, the other two Euler angles undergo only a small net change during each azimuthal period.

In order to remove this short-period oscillation, leaving only the long-period motions, we average the Euler angles over one azimuthal revolution with respect to the s_3-axis, and call the resulting equations *azimuthally-averaged equations*.

To simplify the analysis, the time rates of change of the Euler angles may be written as

$$\frac{d\phi}{d\tau} = A + C_\phi \sin 2\phi + D_\phi \cos 2\phi, \qquad [54a]$$

$$\frac{d\theta}{d\tau} = B + C_\theta \sin 2\phi + D_\theta \cos 2\phi \qquad [54b]$$

$$\frac{d\psi}{d\tau} = C + C_\psi \sin 2\phi + D_\psi \cos 2\phi; \qquad [54c]$$

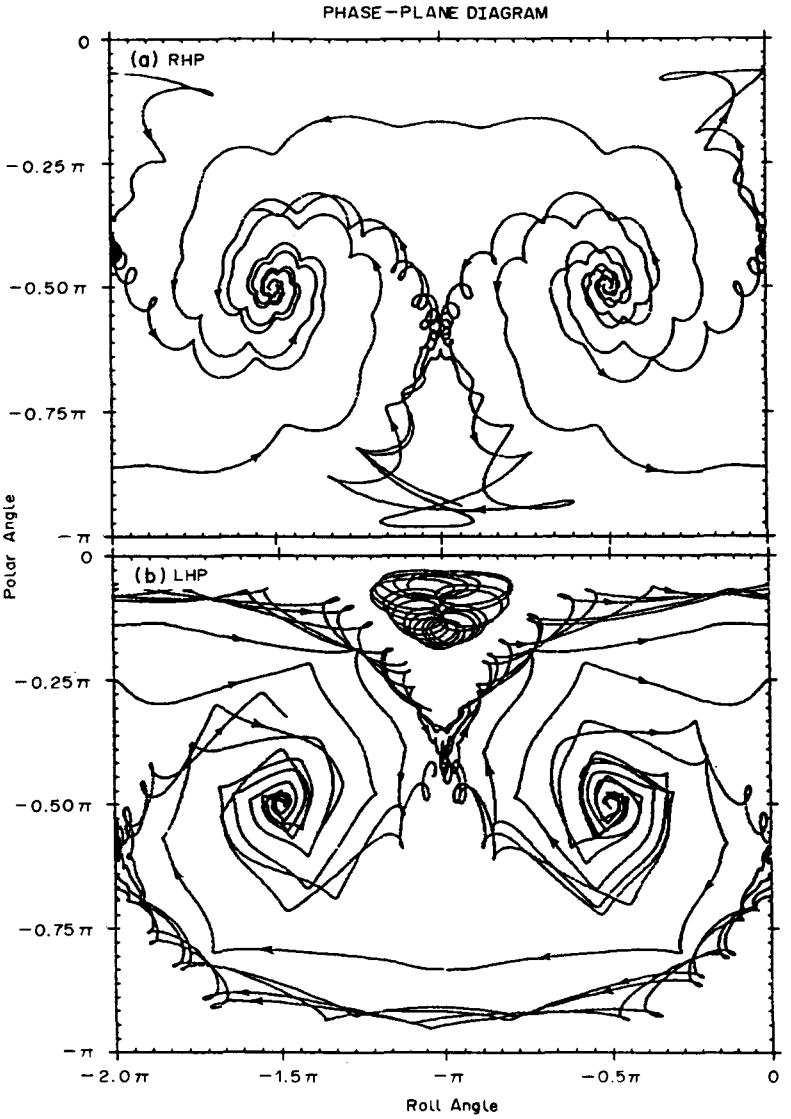

Figure 12. Phase-plane diagram of helical particles for $L/D = 1$, $n = 2$, $d/2a = 0.1$ and $Y = 100$.

in which the coefficients depend on the resistance tensors $\mathbf{B}_c$ and $\mathbf{P}_c$ and Euler angles θ and ψ.

The azimuthally-averaged expression for the polar-angle variation during one azimuthal period P is:

$$\begin{aligned}\Delta\Theta &= \int_0^P \dot{\theta}\, d\tau \\ &= \int_0^{2\pi} \frac{\dot{\theta}}{\omega_{s_3}} d\phi \\ &= \int_0^{2\pi} \frac{B + C_\theta \sin 2\phi + D_\theta \cos 2\phi}{J + E \sin 2\phi + F \cos 2\phi} d\phi. \end{aligned} \quad [55]$$

If the polar- and roll-angle dependences of the above coefficients are neglected, the integral can be carried out in closed form as

$$\Delta\Theta = BP + (2\pi - JP)\frac{C_\theta E + D_\theta F}{H^2}, \quad [56]$$

where

$$J = A + C\cos\theta, \quad E = C_\phi + C_\psi \cos\theta, \quad F = D_\phi + D_\psi \cos\theta, \quad H = \sqrt{E^2 + F^2}; \tag{57}$$

and the quantity P denotes the period of one revolution of the particle with respect to the s_3-axis.

$$P = \int_0^{2\pi} \frac{d\phi}{\omega_{s_3}} = \frac{2\pi}{J\sqrt{1 - \left(\frac{H}{J}\right)^2}}. \tag{58}$$

As the relative importance of gravity increases, a point is reached where the particle rotation due to sedimentation becomes comparable with that induced by the shear flow. At this point, it is possible for a particle of screw sense to settle without rotation, and azimuthal averaging is not valid in this range.

Similarly, the azimuthally-averaged roll-angle variation can be expressed as

$$\Delta\Psi = CP + (2\pi - JP)\frac{C_\psi E + D_\psi F}{H^2}. \tag{59}$$

If we now consider the period P to be a continuous variable describing the long-period motion ($t \gg 2\pi/G$), then the aximuthally-averaged equations can be interpreted as ordinary differential equations, and this makes it possible to use a two-dimensional phase-plane solution.

In order to find the terminal states, we find the loci of $\Theta' = 0$ and $\Psi' = 0$, where the prime denotes d( )/dP. The intersection points of these loci represent the critical points, some of which may be the terminal states. The nature of these points can be determined by standard methods of nonlinear mechanics [see also Andronov *et al.* (1987)].

In a similar manner, the azimuthally-averaged location of the center of mass can be found from

$$\Delta S_{i(i=1,2,3)} = \int_0^P \dot{s}_i \, d\tau = \int_0^{2\pi} \frac{U_{c.m,i}}{\omega_{s_3}} d\phi, \tag{60}$$

where the components of the translational velocity in the space-fixed coordinates $U_{c.m,i}$ are written as:

$$U_{c.m,1} = [A^{I}\sin\phi + B^{I}\cos\phi]Y + C^{I}\sin\phi\sin 2\phi + D^{I}\sin\phi\cos 2\phi + E^{I}\cos\phi\sin 2\phi + F^{I}\cos\phi\cos 2\phi, \tag{61}$$

$$U_{c.m,2} = s_1 + [A^{II}\sin\phi + B^{II}\cos\phi]Y + C^{II}\sin\phi\sin 2\phi + D_{II}\sin\phi\cos 2\phi + E^{II}\cos\phi\sin 2\phi + F^{II}\cos\phi\cos 2\phi, \tag{62}$$

$$U_{c.m,3} = [A^{III}]Y + C^{III}\sin 2\phi + D^{III}\cos 2\phi; \tag{63}$$

in which the coefficients depend on $\mathbf{R}_c$ and $\mathbf{Q}_c$ and Euler angles θ and ψ.

Since $U_{c.m,3}$ is a function of $\sin(2n\phi)$, the integration of S_3 is written in the same form as that of the azimuthally-averaged Euler angles:

$$\Delta S_3 = A^{III}YP + (2\pi - JP)\frac{C^{III}E + D^{III}F}{H^2}. \tag{64}$$

We have been unable to find the closed-form expression for the integrals that give ΔS_1 and ΔS_2, and therefore we have used a Simpson's-rule integration. The leading term in $U_{c.m,2}$ is s_1, and it follows that the azimuthally averaged S_2 velocity is equal to the average value of S_1, i.e.

$$S_2' = S_1. \tag{65}$$

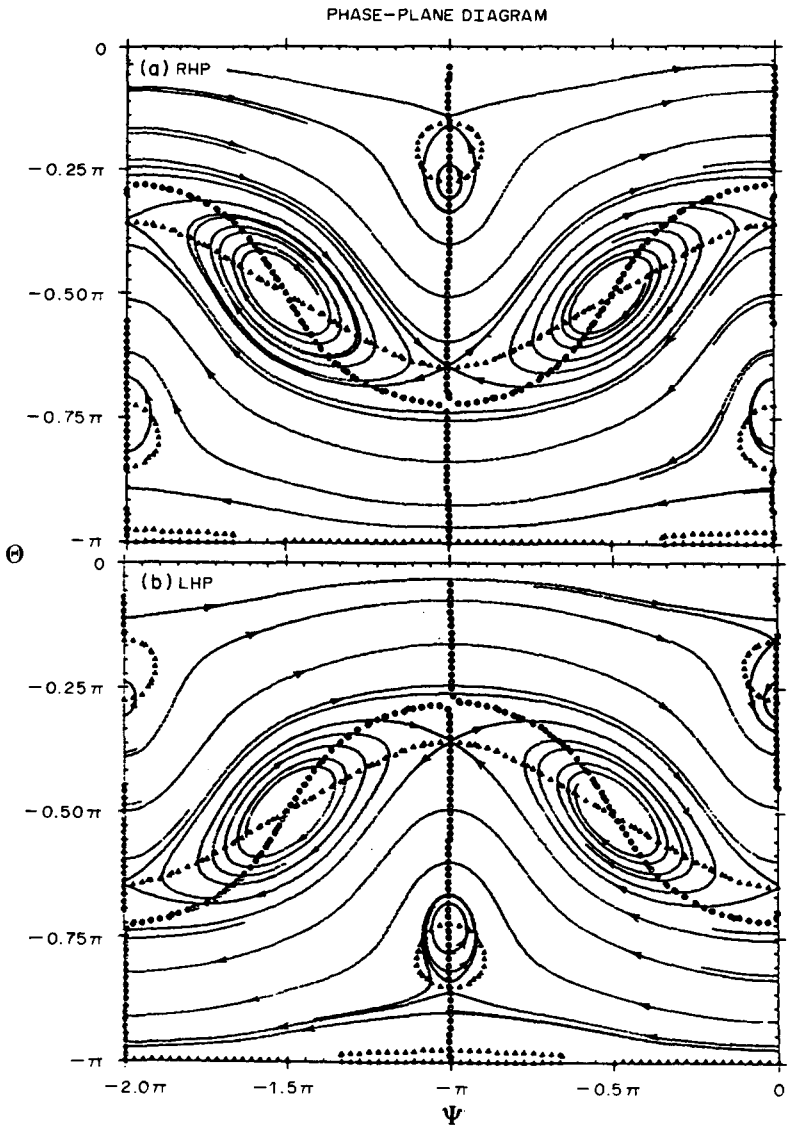

Figure 13. Asimuthally-averaged phase portraits of helical particles for $L/D = 1$, $n = 2$, $d/2a = 0.1$ and $Y = 0$.

In figures 13–15, we show several phase portraits to check the above approximation, where the loci of $\Theta' = 0$ and $\Psi' = 0$ are plotted as circular and triangular symbols, respectively. For a neutrally-buoyant RHP, there are several critical points; for instance, $\Theta/\Psi = -90°/-90°$, $-90°/-270°$ for unstable and stable foci, respectively, and the saddle points are located at Euler angles of $-65°/0°$, $-117°/-180°$.

On the other hand, the phase-plane diagram of a neutrally-buoyant LHP shows a different nature of the critical points: saddle points at $\Theta/\Psi = -65°/-180°$, $-117°/-360°$; and stable, unstable foci at $-90°/-90°$, $-90°/270°$, respectively.

As illustrated in figure 15, the trajectories of heavier particles ($Y = 100$) show the gravity effect on particle motion. In fact, this phase portrait is very similar to that found earlier in the no-shear case [see also figure 13 in Kim & Rae (1989)]. It also shows the *basins of attraction* [Thompson & Stewart 1986) of a couple of terminal states.

6. IMPLICATIONS FOR SEPARATION

The calculations described above can be used to infer some conclusions about the feasibility of separating mixtures of right- and left-handed helical coils. These conclusiosn are of course tempered

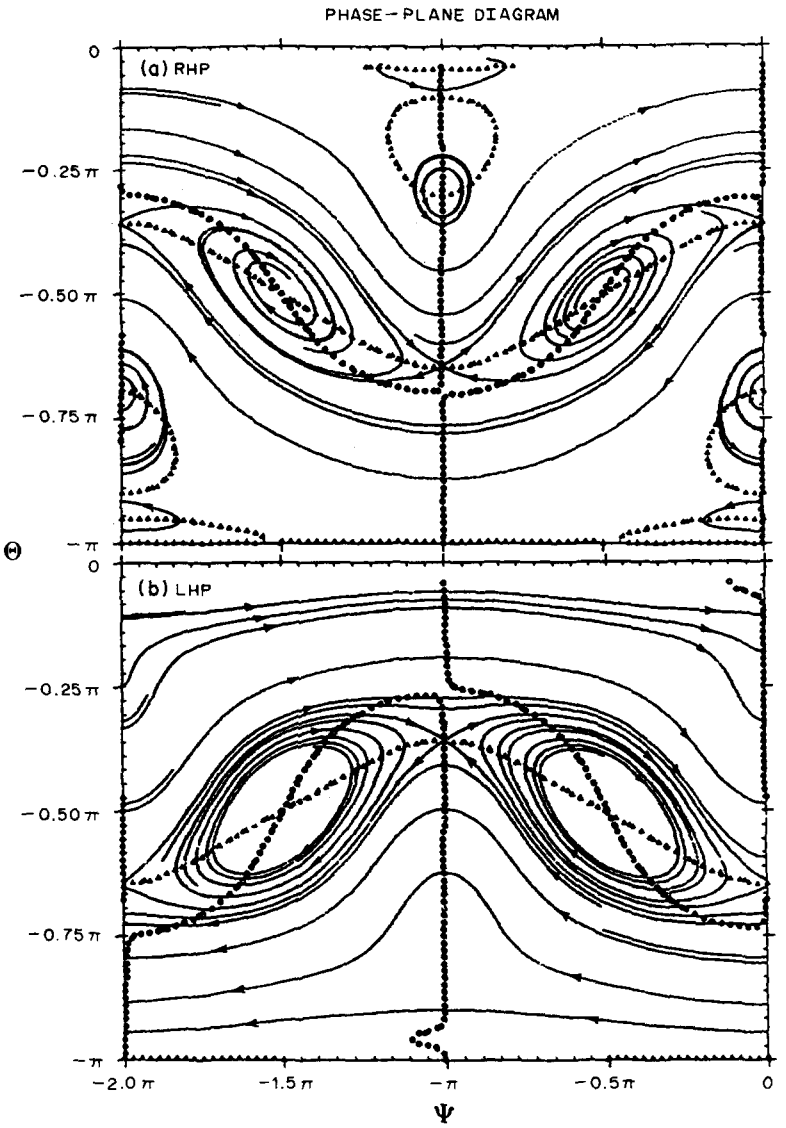

Figure 14. Azimuthally-averaged phase portraits of helical particles for $L/D = 1$, $n = 2$, $d/2a = 0.1$ and $Y = 1$.

by the approximations made, notably the neglect of walls and of interparticle interactions, but the present results may be indicative of what might be expected for a dilute suspension in a concentric-cylinder Couette-flow apparatus whose gap dimension is large compared to the particle scale.

Reliable inferences about separation require knowledge of the terminal motions of the particle, which are approached at large values of τ. The calculations carried out during this work suggest that *large* values of τ are on the order of $\geqslant 10^4$. But τ is 2π times the motion time measured in period of the fluid spin, i.e.

$$\tau = GT = 2\pi \frac{t}{P}; \quad P = \frac{2\pi}{G}.$$

Thus, the motion must be calculated out to some hundreds to thousands of fluid–spin cycles before the terminal orientations and their corresponding translational velocities are evident.

An example of this requirement can be seen in figures 6 and 11: in terms of the concentric-cylinder apparatus, the displacements s_1, s_2 and s_3 correspond, respectively, to the radial, circumferential and vertical directions. While the s_1 and s_2 displacements seen in figure 6 are of no utility for separation, it is tempting to conclude that a long-term separation in the vertical direction is

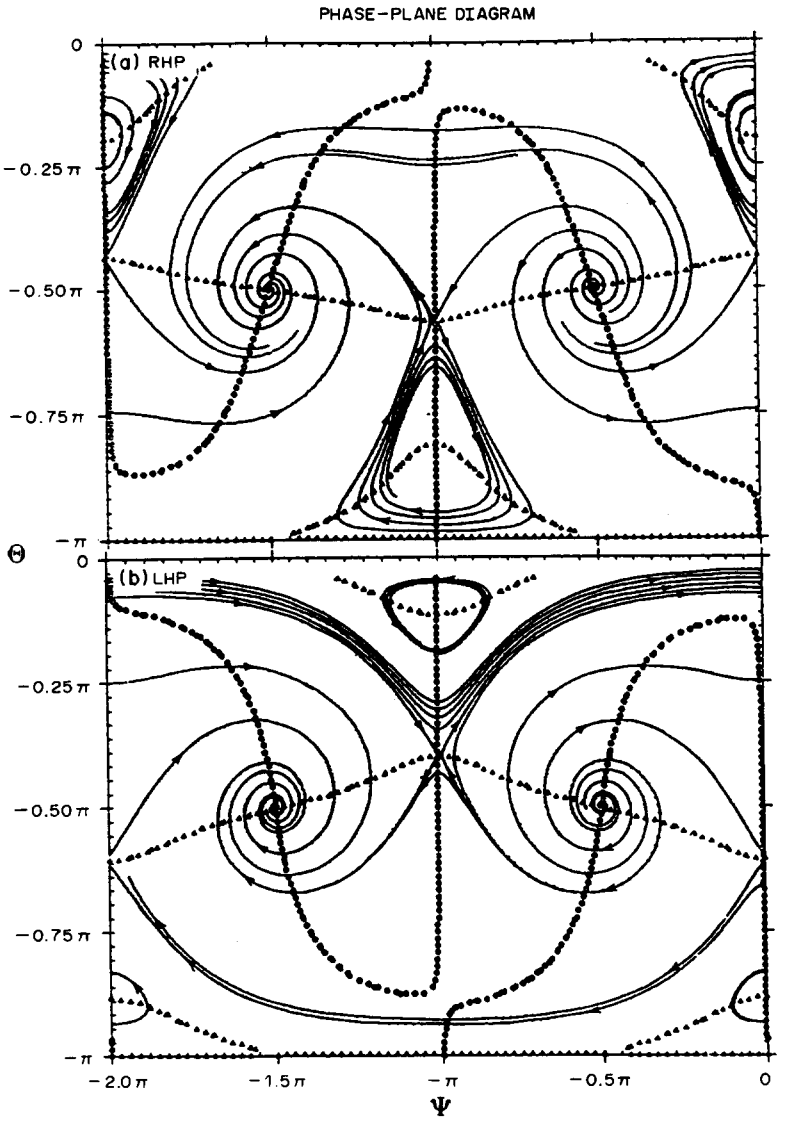

Figure 15. Azimuthally-averaged phase portraits of helical particles for $L/D = 1$, $n = 2$, $d/2a = 0.1$ and $Y = 100$.

possible. However, this steady different drift does not persist out to large times; in fact, examination of the θ, ψ phase portrait for this motion (it is indistinguishable from that for $Y = 1$, shown in figure 11) shows that the initial orientation lies near an unstable focus and that many thousands of cycles later, these particles will approach terminal states having $\theta = -90°$, $\psi = -270°$.‡ The fact that $\tau = 500$ is very early in the motion is confirmed by figure 5, which shows that the polar and roll angles remain within a few degrees of their initial values throughout this time period.

It is at this point that the azimuthally-averaged equations are most valuable, since they enable identification of the terminal states with considerably less computational effort (cf. figure 11 with figures 13 or 14).

‡In this orientation, the central axis of the coil is horizontal, with the ends of the coil *pointing down*, i.e. they are located on the bottom side of the coil. This is the same terminal state seen in the pure-sedimentation results (Kim & Rae 1989) and is different from the −90°, 90° orientation that the present authors' intuition would have suggested. Thus, the cautionary remarks of Kim & Rae (1989) bear repetition here: terminal orientations are quite sensitive to *end effects*, i.e. slight changes in the particle geometry near its ends can have a large effect on terminal orientation. In addition, it should be stressed that the only coil geometry treated in the present paper is one having an integer number of turns, for which the center of mass lies on the coil axis. A limited number of calculations, not reported here, suggest that small off-axis displacements of the center of mass can create large changes in the terminal orientations.

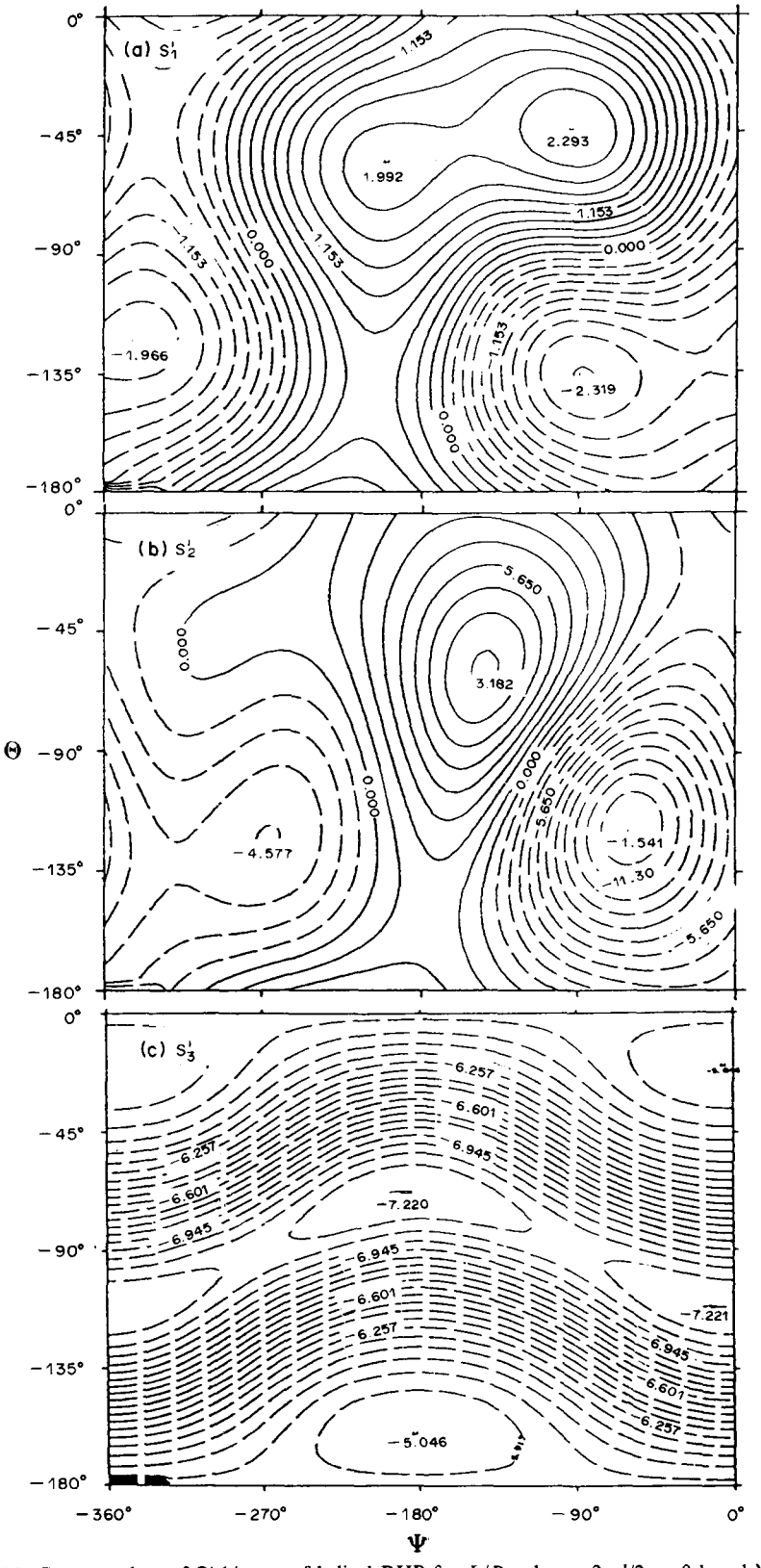

Figure 16. Contour plots of S_1' history of helical RHP for $L/D = 1$, $n = 2$, $d/2a = 0.1$ and $Y = 1$.

Given that $\theta, \psi = -90°, -270°$ is the terminal orientation (with $\dot{\phi} \approx$ const), the time-averaged translational velocities can then be found from figures such as 16 and 17.

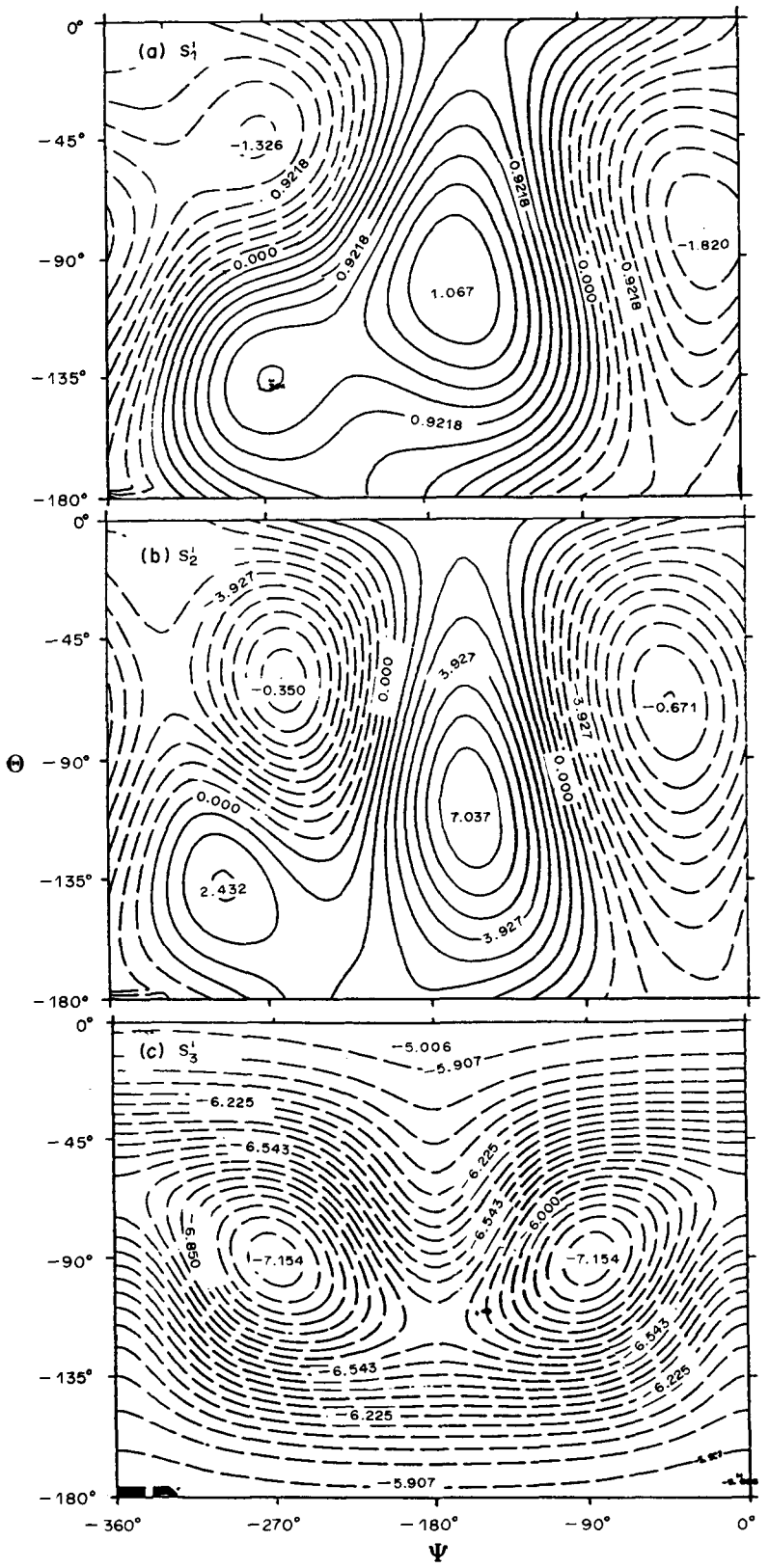

Figure 17. Contour plots of S_1^i history of helical LHP for $L/D = 1$, $n = 2$, $d/2a = 0.1$ and $Y = 1$.

The results shown in table 3 show that particles of near-neutral buoyancy do not show a useful separation in a linear shear flow, but that a differential sedimentation rate does develop for nonneutrally-buoyant particles. This effect is essentially that described in [49]–[53]: at terminal

Table 3. Time-averaged translational velocities of $\theta, \psi = -90°, -270°$ for Y = 1 and Y = 10

	S_1'	S_2'	S_3'
Y = 1			
RHP	0.0206	−4.7275	−7.1382
LHP	0.0440	−2.8155	−7.1576
Y = 10			
RHP	0.0268	−45.5734	−69.2571
LHP	0.0455	−29.5294	−73.8626

conditions, the sedimentation velocity is that of a neutrally-buoyant particle (this part is independent of screw sense) plus or minus a component proportional to Y. The latter is due to the gravity-induced rotation and can either hinder or assist the motion, depending on the handedness. To show this phenomenon, we plot the time-averaged translational velocity along the s_3-direction with various values of the buoyancy parameter Y at $\theta, \psi = -90°, -270°$ in figure 18.

The general conclusion which we reach is that the flow geometry studied here is conducive to a separation of particles of opposite screw sense, and that the methods of analysis developed here facilitate the prediction of this phenomenon. Further numerical study and comparison with carefully designed experiments are needed to define the separative capability of this flow environment.

7. CONCLUDING REMARKS

The motions of three-dimensional screw-shaped slender filaments are examined in the presence of the combined effects of a linear shear flow and gravitational sedimentation. In particular, the particles tend to rotate in unison with the angular rotation of the shear flow, for all orientations. Because the fundamental period for a helical particle of unit-order length-to-diameter ratio is short compared to the long-term drift of the other kinematical variables, it is possible to derive a set of azimuthally-averaged equations containing only two of the Euler angles. This makes possible a phase-plane analysis comparable with that applied earlier by Kim (1987) to the problem of sedimentation in the absence of shear.

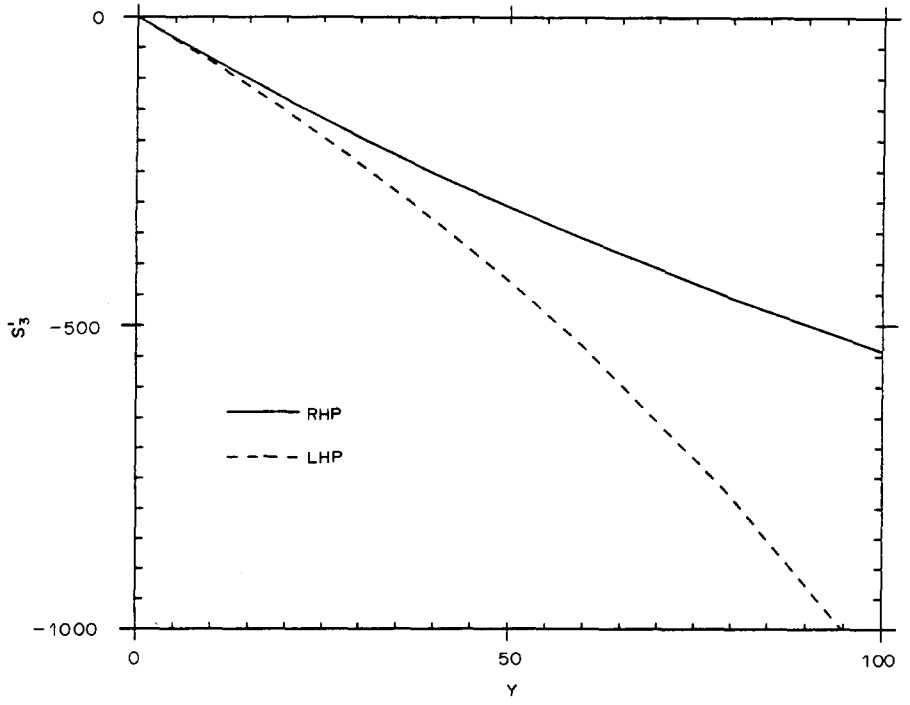

Figure 18. Time-averaged translational velocity along the s_3-direction with various values of the buoyancy parameter Y at $\theta, \psi = -90°, -270°$.

One of the important products of the phase-plane analysis is the ability to predict terminal translational velocities, and hence the potential for achieving separation of screw-sensed particles, without having to endure the extremely long integration times that would be required by the full 6 degrees-of-freedom equations. The results of this analysis, applied to a limited number of cases, make it clear that some separations can occur, and the methods developed here can be used to estimate the overall separation to be expected from dilute racemic suspensions acted on by the combined effects of shear and gravity. Further study is required, to better define the separative capability of this flow geometry, as affected by conditions at the ends of the particle, by off-axis center-of-mass locations, and by further study of effects arising from resistance-tensor elements which are numerically small but nonzero.

The solutions found above are of great value in the applications mentioned earlier, and can serve as the basis for the design of experiments to explore the potential for *separation*. They are also the first step in accounting for a number of more complex phenomena. In particular, effects due to interaction with another particle can easily be examined in the slender-filement approximation (Brown 1990).

A second complication is that of motion in a nonuniform shear field including wall effects, e.g. Poiseuille or Dean flow fields—which, of course, need more resistance coefficients.

Finally, any attempt to apply this work to extremely small particles must deal with the effects of Brownian motion, particle flexibility, end effects, thicker-filament effects and external forces such as those due to electric or magnetic fields.

The problem treated in this paper is a first look at the Stokes-regime motion of a three-dimensional particle, which does not have geometrical symmetries. A great variety of phenomena are found, which are not only of interest in their own right, but are also the first step in illuminating a number of further and more complex problems.

Acknowledgement—The authors are grateful to the referees for many useful comments on this paper.

REFERENCES

ANDRONOV, A. A., VITT, A. A. & KHAIKIN, S. E. 1987 *Theory of Oscillators*, English Language edn (Edited by FISHWICK, W.). Dover, New York.

BATCHELOR, G. K. 1970 Slender-body theory for particles of arbitrary cross-section in Stokes flow. *J. Fluid Mech.* **44,** 419–440.

BRENNER, H. 1964 The Stokes resistance of an arbitrary particle—III. Shear field. *Chem. Engng Sci.* **19,** 631–651.

BRENNER, H. 1966 Hydrodynamic resistance of particles at small Reynolds numbers. In *Advances in Chemical Engineering*, Vol. 6 (Edited by DREW, T. B. *et al*). pp. 287–438. Academic Press, New York.

BROWN, P. C. 1990 Calculation of the motion in Stokes flow of a slender filament helical particle in the vicinity of a wall. M.S. Thesis, State Univ. of New York at Buffalo, N.Y.

BURGERS, J. M. 1938 On the motion of small particles of elongated form suspended in a viscous liquid. *Kon. Ned. Akad. Wet.* **16,** 113–184.

CHWANG, A. T. & WU, T. Y. 1974 Hydromechanics of low-Reynolds number flow, Part 1. Rotation of axisymmetric prolate bodies. *J. Fluid Mech.* **63,** 607–622.

CHWANG, A. T. & WU, T. Y. 1975 Hydromechanics of low-Reynolds number flow, Part 2. Singularity method for Stokes flow. *J. Fluid Mech.* **67,** 787–815.

GOLDSTEIN, H. 1980 *Classical Mechanics*, 2nd edn. Addison-Wesley, Reading, Mass.

JEFFERY, G. B. 1922 The motion of ellipsoidal particles immersed in a viscous fluid. *Proc. R. Soc.* **A102,** 161–179.

JOHNSON, R. E. 1977 Slender-body theory for Stokes flow and flagellar hydrodynamics. Ph.D. Thesis, California Inst. of Technology, Pasadena, Calif.

JOHNSON, R. E. 1980 An improved slender-body theory for Stokes flow. *J. Fluid Mech.* **99,** 411–431.

JOHNSON, R. E. & WU, T. Y. 1979 Hydrodynamics of low-Reynolds number flow, Part 5. Motion of a slender-torus. *J. Fluid Mech.* **95,** 263–277.

KELLER, J. B. & RUBINOW, S. I. 1976 Slender-body theory for slow viscous flow. *J. Fluid Mech.* **75,** 705–714.

KIM, Y.-J, 1987 Calculations of the Stokes-flow resistance matrices for a helical particle, using slender-body theory. MS Thesis, State Univ. of New York at Buffalo, N.Y.

KIM, Y.-J. 1990 Low Reynolds number motion of a helical particle in a linear shear flow. Ph.D. Thesis, State Univ. of New York at Buffalo, N.Y.

KIM, Y.-J. & RAE, W. J. 1989 Stokes-flow sedimentation of a slender-filament helical coil. *PhysicoChem. Hydrodynam.* **11,** 295–314.

STRUIK, D. J. 1950 *Differential Geometry.* Addison-Wesley, Reading, Mass.

THOMPSON, J. M. T. & STEWART, H. B. 1986 *Nonlinear Dynamics and Chaos.* Wiley, New York.

TILLETT, J. P. K. 1970 Axial and transverse Stokes flow past slender axisymmetric bodies. *J. Fluid Mech.* **44,** 401–417.